Efficacy and mechanism of action of cipargamin as an antibabesial drug candidate

Authors

Hang Li[1#], Shengwei Ji[1,2#], Nanang R. Ariefta[1], Eloiza May S. Galon[3], Shimaa AES El-Sayed[1,4], Thom Do[1], Lijun Jia[2], Miako Sakaguchi[5], Masahito Asada[1], Yoshifumi Nishikawa[1], Xin Qin[6], Mingming Liu[6]*, Xuenan Xuan[1]*

Affiliations

[1]National Research Center for Protozoan Diseases, Obihiro University of Agriculture Veterinary Medicine, Inada-cho, Obihiro, Japan

[2]Department of Veterinary Medicine, Agriculture College of Yanbian University, Yanji, China

[3]College of Veterinary Medicine and Biomedical Sciences, Cavite State University, Indang, Philippines

[4]Department of Biochemistry and Molecular Biology, Faculty of Veterinary Medicine, Mansoura University, Egypt

[5]Central Laboratory, Institute of Tropical Medicine (NEKKEN), Nagasaki University, Nagasaki, Japan

[6]School of Basic Medicine, Hubei University of Arts and Science, Xiangyang, China

***Correspondence:** Mingming Liu; Xuenan Xuan

Address: Longzhong Road No.296, Xiangyang, China; Nishi 11 Minami 39 Chome, Obihiro, Hokkaido

Telephone number: +8618904416800; +8109079036369

E-mail address: lmm_2010@hotmail.com; gen@obihiro.ac.jp

Competing interest: The authors have declared that no conflict of interest exists.

# These authors contributed equally to this work.

Abstract

Babesiosis is a disease brought on by intraerythrocytic parasites of the genus *Babesia*. Current chemotherapies are accompanied by side effects and parasite relapse. Therefore, it is crucial to develop highly effective drugs against *Babesia*. Cipargamin (CIP) has shown inhibition against apicomplexan parasites, mainly *Plasmodium* and *Toxoplasma*. This study evaluated the growth-inhibiting properties of CIP against *Babesia* spp. and investigated the mechanism of CIP on *B. gibsoni*. The half inhibitory concentration (IC_{50}) values of CIP against the *in vitro* growth of *B. bovis* and *B. gibsoni* were 20.2 ± 1.4 nM and 69.4 ± 2.2 nM, respectively. CIP significantly inhibited the growth of *B. microti* and *B. rodhaini in vivo.* Resistance was conferred by L921V and L921I mutations in *Bg*ATP4, which reduced the sensitivity to CIP by 6.1- and 12.8-fold. The inhibitory potency of CIP against *Bg*ATP4-associated ATPase activity was moderately reduced in mutant strains, with a 1.3-fold and 2.4-fold decrease in *Bg*ATP4^{L921V} and *Bg*ATP4^{L921I} compared to that of *Bg*ATP4^{WT}, respectively. An *in silico* investigation revealed reductions in affinity for CIP binding to *Bg*ATP4^{L921V} and *Bg*ATP4^{L921I} compared to *Bg*ATP4^{WT}. Resistant strains showed no significant cross-resistance to atovaquone (ATO) or tafenoquine (TQ), with less than a onefold change in IC_{50} values. Combining CIP with TQ effectively eliminated *B. microti* infection in SCID mice, no relapse, and parasite DNA was not detected by qPCR within 90 days post-infection. Our findings reveal the efficacy of CIP as an anti-babesial agent, its limitations as a monotherapy due to resistance development, and the potential of combination therapy with TQ to overcome resistance and achieve complete parasite clearance.

Keywords: Cipargamin; *Babesia* spp.; drug resistance; ATP4; mutation

Introduction

Babesia is an apicomplexan tick-transmitted hemoparasite, which not only impacts the livestock economy but also causes an emerging disease in humans (Jalovecka et al., 2019). *Babesia* is a global pathogen that is more prevalent in certain regions such as Asia, Europe, and North America. However, as climate change brings with it higher temperatures and humidity, ticks and their reservoir hosts are anticipated to expand northward for survival and activity (Gray and Ogden, 2021). The disease is known as babesiosis, commonly characterized by fever and hemolytic anemia, but chronic infections can be asymptomatic (Almazán et al., 2022). The fatality rate ranges from 1% among all cases to 3% among hospitalized cases, and as high as 20% in immunocompromised patients (Krause, 2019).

Currently, the most common drugs for the treatment of human babesiosis include a combination of atovaquone (ATO) plus azithromycin (AZI) or clindamycin (CLN) plus quinine (QUI) (Krause et al., 2021). Still, these recommended treatments often result in various problems. For instance, multiple mutations in the *B. microti* cytochrome b, which is targeted by ATO, were identified in patients with relapsing babesiosis (Holbrook et al., 2023; Krause et al., 2024; Lemieux et al., 2016; Marcos et al., 2022; Rogers et al., 2023; Rosenblatt et al., 2021; Simon et al., 2017). The combination of CLN and QUI is the last resort for patients with severe symptoms (Kletsova et al., 2017). Despite its efficacy, this combination can elicit adverse drug reactions (Vannier and Krause, 2012). The 8-aminoquinoline analog tafenoquine (TQ) was found to be effective in curing immunocompromised patients experiencing relapsing babesiosis caused by *B. microti* (Rogers et al., 2023). However, the efficacy of TQ treatment may vary between individuals and cases and its contraindication in patients with glucose-6-phosphate dehydrogenase (G6PD) deficiency limits its clinical use (Chu and Freedman, 2019). Due to the aforementioned issues, it is undoubtedly urgent to search for compounds that treat infections caused by *Babesia* spp. while simultaneously

74 minimizing the detrimental side effects of antibabesial drugs.

75 Spiroindolone cipargamin (CIP), a promising antimalarial, has been found to effectively
76 suppress the growth of all strains of *Plasmodium falciparum* and *P. vivax* with potency in the
77 low nanomolar ranges (Rosling et al., 2018; Rottmann et al., 2010). The assessment of the
78 drug indicated that CIP taken orally had good absorption, a long half-life, and exceptional
79 bioavailability (Schmitt et al., 2022). Following oral CIP treatment (30 mg daily for three
80 days) in adults with simple *P. falciparum* or *P. vivax* malaria, parasitemia was rapidly cleared
81 in a phase II trial (Schmitt et al., 2022). Currently, a clinical trial is being conducted for the
82 intravenous administration of CIP as a treatment for severe malaria patients (ClinicalTrials,
83 2024). CIP was also evaluated for treating toxoplasmosis as a second-line medicine in cases
84 where there are intolerable toxicity issues or allergies to the currently used treatments. Mice
85 infected with *T. gondii* that were treated with CIP on the day of infection and the following
86 day had 90% fewer parasites five days post-infection (Zhou et al., 2014).

87 *Pf*ATP4, a P-type ATPase in *P. falciparum*, functions as a Na^+/H^+ transporter critical for
88 maintaining ionic balance (Spillman et al., 2013). Mutations in *Pf*ATP4 confer resistance to
89 CIP, which disrupts Na^+ homeostasis, leading to increased cytosolic Na^+ concentration and
90 various physiological changes, such as cytosolic alkalinization, osmotic swelling, etc.
91 (Mohring et al., 2022). These mutations reduce the Na^+-dysregulating effects of CIP and the
92 resting Na^+ levels. While *Pf*ATP4 is essential for *P. falciparum* survival, its homolog in *T.*
93 *gondii* (*Tg*ATP4) is less critical, as *T. gondii* experiences brief, high Na^+ exposure and can
94 survive without *Tg*ATP4 expression (Lehane et al., 2019).

95 Due to its excellent efficacy against other apicomplexan parasites, including *Plasmodium*
96 spp., and its ability to target parasite ATP4—a conserved protein essential for ion homeostasis
97 in apicomplexan organisms—we hypothesize that CIP could also effectively inhibit *Babesia*
98 spp., a related apicomplexan parasite. Therefore, the objectives of this study were to

99 determine whether CIP could inhibit the growth of *Babesia* spp., namely *B. bovis* and *B.*
100 *gibsoni in vitro* and *B. microti* and *B. rodhaini in vivo*, and identify the inhibitory mechanisms
101 of CIP on *Babesia* parasites.
102
103 **Results**
104 **Inhibitory efficacy of CIP on *B. bovis* and *B. gibsoni in vitro***
105 *In vitro* efficacy of CIP against *B. bovis* and *B. gibsoni* showed a steep growth inhibition
106 curve with half inhibitory concentration (IC_{50}) values of 20.2 ± 1.4 nM (Figure 1A) and 69.4
107 ± 2.2 nM (Figure 1B), respectively. The 50% cytotoxic concentration (CC_{50}) value of CIP on
108 Madin-Darby canine kidney (MDCK) cells and human foreskin fibroblasts (HFF) were 38.7
109 ± 2.0 μM and 70.8 ± 4.9 μM (Figure supplement 1), respectively. Based on these values, the
110 predicted selectivity indices (SIs), which reflect the drug's safety and specificity, were
111 calculated to be greater than 500. Furthermore, at a concentration of 100 μM, CIP exhibited a
112 low erythrocyte hemolysis rate of 0.11 ± 0.03 % (data not shown).
113 **CIP effect on *B. microti* and *B. rodhaini* infections *in vivo***
114 Concurrently, CIP showed effective inhibition on *B. microti* and *B. rodhaini in vivo*. The
115 parasitemia of *B. microti*-infected BALB/c mice increased dramatically in the vehicle-treated
116 control group and peaked at 10 days postinfection (DPI) (38.55 ± 4.32%) (Figure 1C). On the
117 other hand, seven days of treatment with CIP (20 mg/kg) or atovaquone (ATO) plus
118 azithromycin (AZI) administered orally resulted in a significantly lower peak parasitemia,
119 1.06 ± 0.20% and 1.61 ± 0.20%, respectively (Figure 1C). Hematocrit (HCT) variations were
120 tracked every 4 days as an indicator of anemia in *B. microti*-infected mice. The
121 vehicle-treated group showed a drop in HCT levels at 12 DPI and 16 DPI ($P < 0.01$) (Figure
122 1D). No significant reduction in HCT levels was observed in the CIP-treated group or the
123 ATO plus AZI-treated group (Figure 1D). This indicates that the administration of CIP could

124 control *B. microti* infection and prevent anemia from developing in *B. microti*-infected mice.
125 BALB/c mice infected with *B. rodhaini* treated with sesame oil or ATO plus AZI showed high
126 parasitemia, 90.73 ± 1.97%, and 86.23 ± 3.06%, respectively (Figure 1E), and all mice died
127 within 8 DPI (Figure 1F). CIP treatment in *B. rodhaini*-infected mice precluded the
128 emergence of parasitemia for the following eight days (Figure 1E), which led to 66.67% of
129 mice surviving the challenge infection (Figure 1F). At 12 DPI, parasites had recurred in all
130 CIP-treated *B. rodhaini*-infected mice (10.32 ± 15.51%), which were eventually cleared as
131 indicated by undetectable parasites at 18 DPI (Figure 1E).

132 **Identification of *B. gibsoni* ATP4 mutation in CIP-resistant strains**

133 After being exposed to CIP at increasing concentrations up to 10 times the IC_{50}, the resistant
134 parasites in two of the culture wells were able to regrow. We sequenced the *B. gibsoni* ATP4
135 gene from the wild-type and two resistant strains. The wild-type strain has a C at nucleotide
136 2,761, which translates to leucine (Figure 2A). In one resistant strain, a single nucleotide
137 variant (SNV) in *Bg*ATP4 with a substitution at position 2,761 (from C to G) was found − a
138 nonsynonymous coding change from leucine to valine (L921V) (Figure 2B). In another
139 resistant strain, the mutation occurred in the same position. However, the nucleotide
140 substitution was from C to A, and the coding changed from leucine to isoleucine (L921I)
141 (Figure 2C). Next-generation sequencing (NGS) revealed that for *Bg*ATP4^{L921V}, 99.97% of
142 7,960 reads were G at nucleotide 2,761, and for *Bg*ATP4^{L921I}, 99.92% of 7,862 reads were A
143 at nucleotide 2,761 (Figure 2D). *Bg*ATP4^{L921V} and *Bg*ATP4^{L921I} lines were tested for their
144 susceptibility to CIP, and had IC_{50} values of 421.0 ± 15.9 nM and 887.9 ± 62.0 nM,
145 respectively (Figure 2E). These findings demonstrate a 6.1- and 12.8-fold reduction in CIP
146 sensitivity of the resistant parasite lines *Bg*ATP4^{L921V} and *Bg*ATP4^{L921I}.

147 **The effect of CIP on *Bg*ATP4^{WT}, *Bg*ATP4^{L921V} and *Bg*ATP4^{L921I} function**

148 Microscopic observation of thin blood smears was performed to determine the morphological

149 changes of *B. gibsoni* exposed to CIP. The CIP-treated parasites became swollen after
150 incubation with the drug for 72 h (Figure 3A). For both the treatment and control groups, one
151 hundred parasites were measured. The mean size of treated parasites was notably bigger than
152 the parasites in the untreated group ($P < 0.0001$) (Figure 3B). Significant vacuolization was
153 observed in the cytoplasm of parasites in the CIP-treated group, as revealed by transmission
154 electron microscopy (TEM). Despite this, the nuclear membrane structure and parasitic
155 membranes remained intact until the parasites were completely destroyed (Figure 3C). The
156 addition of the ATP4 inhibitor CIP resulted in a time-dependent increase in the concentrations
157 of $[Na^+]_i$ in wild-type *B. gibsoni*, with improved signal-to-noise ratios at the higher drug
158 concentration of 20 nM (Figure 3D). We observed that the Na^+ concentrations in both
159 *Bg*ATP4^{L921V} and *Bg*ATP4^{L921I} lines were lower when compared with those of the control
160 *Bg*ATP4^{WT} line after being exposed to 20 nM CIP for 20 min, with a significantly lower Na^+
161 concentration in *Bg*ATP4^{L921I} ($P = 0.0087$) (Figure 3F). We also demonstrated here that the
162 addition of CIP in wild-type *B. gibsoni* caused an increase in the cytosolic pH (Figure 3E).
163 Specifically, 4 min after the drug was added, the average pH of 20 nM CIP group reached as
164 high as 7.278, while the 1 nM CIP group reached 7.089 and the untreated group reached
165 7.062 (Figure 3E). The pH values of the 20 nM CIP group were consistently higher than those
166 of the other two groups, although declining with time (Figure 3E). In resistant lines, a 20-min
167 exposure to 20 nM CIP caused small changes in the pH values compared to the wild-type line,
168 with the *Bg*ATP4^{L921I} line (7.048 ± 0.042) having a notably lower pH value ($P = 0.0229$)
169 (Figure 3G).

170 **Sensitivity of *Bg*ATP4-associated ATPase activity to CIP in *Bg*ATP4^{WT}, *Bg*ATP4^{L921V}**
171 **and *Bg*ATP4^{L921I}**

172 The *Bg*ATP4-associated ATPase activity in erythrocytes infected with *Bg*ATP4^{WT} (6.31 ±
173 1.20 nmol Pi/mg protein/min), measured in the presence of 150 mM Na^+, was higher than that

174 observed in *Bg*ATP4^{L921V} (5.11 ± 0.50 nmol Pi/mg protein/min) and *Bg*ATP4^{L921I} (4.58 ± 0.53
175 nmol Pi/mg protein/min) (P = 0.04) (Figure 3H).
176 We further investigated the concentration-dependent inhibition of *Bg*ATP4-associated ATPase
177 activity by CIP in wild-type and mutant parasites. In membranes prepared from *B.gibsoni*,
178 CIP inhibited *Bg*ATP4-associated ATPase activity with IC_{50} values of 111.4 ± 31.8 nM for
179 *Bg*ATP4^{WT}, 149.8 ± 21.7 nM for *Bg*ATP4^{L921V}, and 269.5 ± 29.8 nM for *Bg*ATP4^{L921I}. The
180 potency of CIP in inhibiting *Bg*ATP4-associated ATPase activity was reduced by 1.3-fold and
181 2.4-fold in membranes prepared from *Bg*ATP4^{L921V} and *Bg*ATP4^{L921I}, respectively, compared
182 to *Bg*ATP4^{WT} (Figure 3I).

183 **Multiple sequence alignment of *Babesia* ATP4 and molecular docking**

184 The whole amino acid sequence of *B. gibsoni* ATP4 (GenBank: KAK1443404.1) shared
185 identity values of 29.75%, 49.40%, 49.67%, 62.21%, and 52.47% with *Homo sapiens* ATP4
186 (GenBank: NM_000704.3), *P. falciparum* ATP4 (GenBank: PF3D7_1211900), *T. gondii*
187 ATP4 (GenBank: XP_018635122.1), *B. bovis* ATP4 (PiroplasmaDB: BBOV_IV010020), and
188 *B. microti* ATP4 (GenBank: BMR1_03g01005), respectively (Figure supplement 2).
189 The pLDDT (predicted Local Distance Difference Test) value of *Bg*ATP4^{WT} prediction was
190 80.7 using Colab-fold. Multiple potential binding sites for CIP were revealed by blind
191 docking throughout the whole protein surface (Figure supplement 3). CIP binds in close
192 proximity to L921, as demonstrated by focused docking on this area (Figure 4A). The
193 contribution of each residue to the predicted binding affinity in either mutant structure was
194 reduced; the precise values of *Bg*ATP4^{WT} (Figure 4B), *Bg*ATP4^{L921V} (Figure 4C), and
195 *Bg*ATP4^{L921I} (Figure 4D) were -6.43, -6.40 and -6.26 kcal/mol, respectively. The interactions
196 of CIP from each docking simulation are shown in Table supplement 3.

197 **Cross-resistance of *Bg*ATP4^{L921V} and *Bg*ATP4^{L921I} mutants to ATO and TQ**

198 The *Bg*ATP4^{WT}, *Bg*ATP4^{L921V}, and *Bg*ATP4^{L921I} lines were tested for their susceptibility to

199 ATO and TQ. The IC_{50} values for these lines were 380.1 ± 3.1 nM, 412.9 ± 5.4 nM, and 360.3
200 ± 7.9 nM, respectively, for ATO (Figure 5A), and 39.5 ± 0.4 μM, 29.9 ± 1.4 μM, and 39.3 ±
201 0.3 μM, respectively, for TQ (Figure 5B). The IC_{50} values for both ATO and TQ in the
202 resistant strains showed only slight changes compared to the wild-type strain, with less than a
203 onefold difference. This minimal variation suggests that the resistant strain has a mild
204 alteration in susceptibility to ATO and TQ, but not enough to indicate strong resistance or
205 significant cross-resistance.

206 **Combination treatment of CIP plus TQ in SCID mice with *B. microti* infection**

207 The parasitemia of *B. microti*-infected SCID mice in the vehicle group increased dramatically,
208 peaking at 10 DPI (77.03 ± 2.45%) (Figure 5C). Although the trend showed a subsequent
209 decline, the parasitemia remained around 50% until the mice were euthanized at 90 DPI.
210 Treatment with CIP (20 mg/kg) initially reduced parasitemia to undetectable by 18 DPI.
211 However, a relapse occurred, with parasitemia increasing rapidly and stabilizing at levels
212 comparable to the vehicle group during the subsequent observation period. Notably, no
213 mutations were detected in the relapsed *B. microti* parasites from SCID mice (data not
214 shown). In contrast, parasitemia was completely cleared in the TQ and CIP plus TQ groups
215 by 8 DPI and 6 DPI, respectively, with no parasites observed under the microscope thereafter.
216 Absolute qPCR analysis at 90 DPI detected parasite DNA in all groups except the CIP plus
217 TQ group (Figure 5D).

218 **Discussion**

219 The repositioning of antimalarial drugs is critical in developing novel strategies for treating
220 babesiosis. CIP is a novel compound that inhibits *Plasmodium* development by targeting
221 ATP4 and has been extensively tested in Phase 1 and Phase 2 clinical trials (Qiu et al., 2022).
222 Since ATP4 is conserved across apicomplexans, including *Babesia* species, our study aimed
223 to repurpose the antimalarial CIP by assessing its efficacy on *Babesia* species (Lehane et al.,

224 2019). The IC_{50} values of CIP against *B. bovis* and *B. gibsoni in vitro* were lower than the
225 previously reported IC_{50} value of TQ (Carvalho et al., 2020; Ji et al., 2022b) and ATO against
226 *B. gibsoni* (Matsuu et al., 2004). The present investigation also demonstrated that the
227 inhibitory effects of CIP on *B. microti*-infected BALB/c mice were comparable to that of
228 ATO plus AZI, the combination recommended by the CDC in the United States. CIP was also
229 proven to protect mice from the deadly *B. rodhaini* infection, with survival up to 67%, as
230 recorded in the current trial. These results suggest that CIP may be a potential chemotherapy
231 candidate for babesiosis.

232 In a previous study, the *P. falciparum* Dd2 strain that acquired resistance to CIP carried the
233 G358S mutation in the *Pf*ATP4 protein, a *P. falciparum* P-type Na^+ ATPase (Qiu et al., 2022).
234 The vital protein ATP4 is found in the parasite plasma membrane and is specific to the
235 subclass of apicomplexan parasites (Mohring et al., 2022). To date, *in vitro* evolution
236 experiments using CIP have produced at least 18 parasite lines with various *Pf*ATP4
237 mutations (Lee and Fidock, 2016; Rottmann et al., 2010). In another study involving *T.*
238 *gondii*, a cell line that carried the mutation G419S in the *Tg*ATP4 gene was 34 times less
239 susceptible to CIP than that of *Tg*ATP4^{WT} (Qiu et al., 2022). It follows that there is a
240 significant chance that the resistant *Babesia* parasites will also emerge from CIP exposure. In
241 this study, we successfully produced two CIP-resistant strains using six independent
242 selections. The newly discovered L921V and L921I mutations in *Bg*ATP4 decreased the CIP
243 sensitivity by 6.1 and 12.8 times, respectively. We provided compelling evidence that natural
244 variety mutations L921V and L921I in *Bg*ATP4 significantly affected the protein's
245 susceptibility to CIP inhibition, albeit the mutational sites were different from those of *P.*
246 *falciparum* and *T. gondii*. Based on our observation, the growth and generation rates of the
247 mutant strains are comparable to those of the wild-type strain.

248 Although ATP4 was initially recognized as a Ca^{2+} transporter (Krishna et al., 2001), current

249 evidence suggests that ATP4 functions as an ATPase for exporting Na^+ while importing H^+
250 (Mohring et al., 2022), as well as causing a variety of other physiological perturbations
251 including an increase in the volume of parasites and infected erythrocytes, due to the osmotic
252 impact of the $[Na^+]_{cyt}$ increase (Dennis et al., 2018), a decline in cholesterol extrusion from
253 the parasite plasma membrane as a result of the increase in $[Na^+]_{cyt}$ (Das et al., 2016), and an
254 intensified rigidity of erythrocytes infected with ring-stage parasites (Zhang et al., 2016). In
255 this study, the CIP-exposed wild-type *B. gibsoni* became swollen, which was identical to a
256 prior study on *P. falciparum* (Dennis et al., 2018). Interestingly, TEM analysis of parasites
257 incubated with CIP revealed ultrastructural alterations characterized by significant vacuole
258 formation in the cytoplasm, a hallmark of stress or early stages of cell death. These changes
259 were similar to those observed in *B. bovis* treated with clotrimazole and ketoconazole, which
260 ultimately led to growth inhibition or parasite death (Bork et al., 2003). Despite the
261 vacuolization, the structural integrity of the nucleus and membranes was maintained,
262 suggesting a gradual process where vacuolization precedes the complete destruction of the
263 parasite. One explanation is the swelling of the isolated parasites, which can be ascribed to
264 the osmotic consequences of Na^+ uptake and is contingent upon the presence of Na^+ in the
265 external environment.

266 The output of Na^+ and input of H^+ diminished upon CIP-induced inhibition of *Pf*ATP4, and
267 the continued outflow of H^+ via V-type H^+-ATPase led to an alkalinization that ultimately
268 killed the parasites (Spillman et al., 2013). Our capacity to measure a time-dependent
269 increase in the concentration of $[Na^+]_i$ and pH value for wild-type *B. gibsoni* facilitated us to
270 gain insight into the basic mechanisms of CIP on *Bg*ATP4^{WT} function. Furthermore, our
271 results validate that internal alkalinization was the main factor in *Babesia* death and support
272 our hypothesis that the swollen isolated parasites were produced by Na^+ absorption. To
273 explore further how mutations in *Bg*ATP4 are associated with the upregulation of the

274 parasite's $[Na^+]_i$ and $[H^+]_i$, we tested two *Bg*ATP4-mutant lines that were chosen previously
275 with *Bg*ATP4 inhibitors (*Bg*ATP4^{L921V} and *Bg*ATP4^{L921I}). Due to the presence of L921V and
276 L921I mutations in drug-resistant strains of *Bg*ATP4, the concentration of Na^+ did not
277 increase as much as it would have in the wild-type strain following the addition of 20 nM CIP
278 for 20 min. As intraerythrocytic alkalinization rises, the same outcome happens. From these
279 results, we deduced how natural mutations in *Bg*ATP4 may affect ATP4 inhibitor
280 susceptibility by dysregulating H^+ and Na^+ balance, which helped parasites survive in a
281 relatively high concentration of CIP. An illustration of the putative processes for regulating
282 Na^+ and H^+ in erythrocytes infected with the *Babesia* parasite is presented in Figure
283 supplement 4.

284 In a previous study's isolated membrane assay, CIP was found to be more effective at
285 inhibiting parasite development than *Pf*ATP4-associated ATPase activity and reduced
286 sensitivity of *Pf*ATP4-associated ATPase activity to the medication was associated with a
287 decrease in parasite susceptibility to CIP (Rosling et al., 2018). In our study, the higher
288 resistance to CIP-mediated inhibition of parasite proliferation observed in *Bg*ATP4^{L921I}
289 compared to *Bg*ATP4^{L921V} correlated with a higher resistance of *Bg*ATP4-associated ATPase
290 activity to the drug. These findings provide additional evidence that the ATPase activity
291 measured in this study corresponds to the activity of the *Bg*ATP4 protein.

292 According to studies using the *Pf*ATP4 model for molecular docking, the G358S mutation
293 results in a steric clash that lowers CIP's binding affinity (Qiu et al., 2022). The results from
294 the current study were similar to the *Pf*ATP4 model. The molecular docking was constructed
295 using a ColabFold model of wild-type *Bg*ATP4, which predicted the binding mode and
296 affinity between ATP4 protein and the ligand to provide a possible mechanistic explanation. It
297 suggested that the L921V mutation caused changes at the atomic level, whereas the L921I
298 mutation created a steric clash that reduced the binding affinity of CIP. The predicted affinity

299 score of the L921I mutation was lower than that of the L921V mutation. Thus, it is possible
300 that CIP had a weaker binding to *Bg*ATP4^{L921I} than to *Bg*ATP4^{L921V}. These findings are
301 consistent with the results obtained from measuring the IC_{50} of the drug against parasites with
302 the L921V and L921I mutations.

303 While CIP shows promise as an antibabesial agent, the emergence of resistance emphasizes
304 the importance of rational drug use and the development of combination therapies. Our
305 results demonstrate that CIP did not exhibit cross-resistance with ATO or TQ, as IC_{50} values
306 for ATO and TQ in resistant strains showed minimal changes (<1-fold) compared to the
307 wild-type strain. This observation suggests that CIP could be effectively combined with other
308 anti-babesial drugs to reduce the risk of resistance development. Previous studies have also
309 reported that a single dose of TQ may not be sufficient to prevent parasite relapse in
310 immunocompromised hosts, recommending either repeated TQ administration or
311 combination therapy with other antibabesial agents to address this issue (Liu et al., 2024).
312 Supporting this approach, our study demonstrates that the combination of CIP plus TQ
313 effectively cleared *B. microti* infections in SCID mice, with no detectable parasitemia or
314 DNA observed at 90 DPI, indicating complete parasite elimination.

315 This preclinical finding underscores the potential of the CIP plus TQ combination as a
316 viable treatment strategy for babesiosis, especially in cases where monotherapy is ineffective.
317 Further studies are needed to fully explore the pharmacokinetics, long-term efficacy, and
318 potential side effects of such combinations in clinical settings, ultimately facilitating
319 optimized therapeutic strategies.

320 In summary, our findings provide a comprehensive understanding of CIP's efficacy,
321 mechanism of resistance, and identifying strategies to enhance its therapeutic potential. The
322 combination of CIP with drugs like TQ offers a promising approach to combat babesiosis and
323 mitigate the development of resistance.

324

325 **Materials and methods**

326 **Parasite culture**

327 The parasites *B. gibsoni* Oita strain and *B. bovis* Texas strain were *in vitro* cultured in 24-well
328 plates and maintained in an atmosphere of 5% CO_2 and 5% O_2 at 37 °C (Liu et al., 2018). For
329 the *in vivo* studies, *B. microti* Peabody mjr strain-(ATCC PRA-99™) and *B. rodhaini*
330 Australia strain-infected RBCs (iRBCs), which were collected and diluted with
331 phosphate-buffered saline (PBS) when the parasitemia levels in the donor mice reached
332 ~20% and 50%, respectively, and were intraperitoneally injected into BALB/c mice. Each
333 BALB/c mouse was infected with 1.0×10^7 *B. microti* or *B. rodhaini* iRBCs for the *in vivo*
334 trials (Ji et al., 2022a).

335 ***In vitro* cytotoxicity of CIP and hemolysis rate in canine erythrocytes**

336 Cultures of Madin-Darby canine kidney (MDCK) cells and human foreskin fibroblasts (HFF)
337 were maintained at 37 °C under an atmosphere of 5% CO_2 and 5% O_2 and the cytotoxic effect
338 of CIP (MedChem Express, Tokyo, Japan) was assessed using a cell viability assay by CCK-8
339 (Dojindo, Japan) as described previously (Li et al., 2023). The selectivity index is calculated
340 as the ratio between the half maximal inhibitory concentration (IC_{50}) and the 50% cytotoxic
341 concentration (CC_{50}) values.

342 Canine erythrocytes were collected from healthy beagle dogs raised in NRCPD and stocked
343 in Vega y Martinez (VYM) phosphate-buffered saline solution at 4 °C (Vega et al., 1985). A
344 canine erythrocyte hemolysis assay was performed at concentrations of 0.1, 1, 5, 10, 25, 50,
345 and 100 μM as previously described (Ariefta et al., 2022).

346 **Evaluation of the efficacy of CIP against *Babesia* parasites *in vitro***

347 The efficacy of CIP against *B. gibsoni* and *B. bovis* was determined using a fluorescence
348 assay, as previously described (Guswanto et al., 2014). The IC_{50} values were determined from

349 the fluorescence values and by non-linear regression analysis (curve fit) in GraphPad Prism 9
350 (GraphPad Software Inc., USA).

351 **Chemotherapeutic effects of CIP against *Babesia* infections *in vivo***

352 CIP was evaluated on *B. microti*- and *B. rodhaini*-infected mice, as previously described
353 (Ndayisaba et al., 2021; Tuvshintulga et al., 2022). When *B. microti*- and *B. rodhaini*-infected
354 mice had a 1% average parasitemia at 4 and 2 days postinfection (DPI), respectively, the drug
355 treatments were administered and continued for seven days. Three groups of *B.*
356 *microti*-infected mice were administered different treatments. The CIP group (n = 6) and the
357 ATO plus AZI group (n = 6) were orally treated with 20 mg/kg CIP and 20 mg/kg ATO plus
358 20 mg/kg AZI (Sigma, Tokyo, Japan), respectively. All drugs were prepared in sesame oil.
359 The infected mice of the vehicle group (n = 6) orally received 0.2 mL of sesame oil as the
360 control. Eighteen mice infected with *B. rodhaini* were likewise placed into three groups for
361 treatment, and they received the same treatments as the mice infected with *B. microti*. A light
362 microscope (Nikon, Japan) and a hematology analyzer (Celltac α MEK-6450, Nihon Kohden
363 Corporation, Tokyo, Japan) were used to assess the parasitemia and hematocrit levels every
364 two and four days, respectively.

365 **Selection of CIP-resistant *B. gibsoni in vitro***

366 Selections were initiated by exposing six independent flasks, each containing 10 μL (5×10^6)
367 *B. gibsoni* iRBCs mixed with 40 μL (4×10^8) RBCs into a 450 μL culture medium, which
368 contained increasing concentrations of CIP: 5, 10, 20, 30 to 694 nM ($10\times IC_{50}$). The medium
369 containing CIP was replaced daily until parasites treated with $10\times IC_{50}$ CIP reached
370 multiplication rates that were approximately comparable to those of the untreated controls
371 (Hwang et al., 2010). Then, to evaluate the decreased sensitivity to CIP, IC_{50} values of
372 resistant strains were determined by nonlinear regression using the GraphPad Prism software.

373 **Detection of *B. gibsoni* ATP4 gene mutations**

374 The genomic DNA of the mutant parasites was extracted and sequenced (Ji et al., 2022a). The
375 primer sets used for sequencing are listed in Table supplement 1. The single nucleotide
376 variants were identified by pairwise alignment to the *Bg*ATP4^{WT} sequence (GenBank:
377 JAVEPI010000002.1). Next-generation sequencing (NGS) was performed to detect the ratio
378 of wild-type to mutant parasites by using the Illumina NovaSeq6000 sequencing platform
379 (Jeon et al., 2021).

380 **Morphological changes in CIP-treated *in vitro* cultured *B. gibsoni***

381 A microscopy assay was used to detect the morphological changes of wild-type *B. gibsoni*
382 after exposure to 50 nM CIP for three consecutive days (Liu et al., 2021; Tayebwa et al.,
383 2018). At 4 days post-treatment, ImageJ software was used to measure the sizes of 100
384 randomly selected parasites in the CIP-treated group and the control group on Giemsa-stained
385 blood smears. After treating the parasites as described above, iRBCs were fixed in GA
386 fixation buffer (2% glutaraldehyde in 0.1 M sodium cacodylate buffer containing 1 mM
387 $CaCl_2$ and 1 mM $MgCl_2$), then stored in rinse buffer (0.1 M sodium cacodylate buffer
388 containing 1 mM $CaCl_2$ and 1 mM $MgCl_2$) at 4 ºC for transmission electron microscopy
389 (TEM) analysis (Hidayati et al., 2023).

390 **Parasites $[Na^+]_i$ and pH_i measurements**

391 For both $[Na^+]_i$ and pH_i measurements, the wild-type and mutant parasites were initially
392 separated from erythrocytes by treatment with saponin (0.05% [wt/vol]) for 5 min (Saliba and
393 Kirk, 1999). The Na^+-sensitive fluorescent dye SBFI (Thermo Fisher Scientific; product
394 S1263) was used to quantify intracellular sodium ($[Na^+]_i$). Saponin-isolated parasites (at
395 1×10^8 parasites/mL) were loaded with SBFI (5 μM; in the presence of 0.02% w/v Pluronic
396 F127) for 1 hr at room temperature (RT) (Spillman et al., 2013). Thereafter, SBFI-loaded
397 parasites were resuspended in physiological saline (120 mM NaCl, 5 mM KCl, 25 mM
398 HEPES, 20 mM D-glucose, and 1 mM $MgCl_2$ [pH 7.1]) at RT in the presence or absence of

399 CIP. A 96-well microtiter plate was filled with around 200 μL of parasite suspension per well.
400 The dye-loaded cells fluoresced at 515 nm after being stimulated at 340 and 380 nm.
401 Parasites loaded with SBFI were suspended in calibration buffers containing [Na^+] values
402 ranging from 0 to 140 mM (pH 7.1) to establish calibration curves (Diarra et al., 2001).
403 The cytosolic pH of wild-type and mutant strains was measured using the pH-sensitive
404 fluorescent dye BCECF [2',7'-bis-(2-carboxyethyl)-5-(and-6)- carboxyfluorescein] (Biotium;
405 product 51011). The BCECF was added to saponin-isolated parasites by suspension (1×10^8
406 parasites/mL) and incubated for 20 minutes at 37 °C in RPMI-1640 culture medium (Gibco,
407 USA) (Saliba and Kirk, 1999). Thereafter, the parasites loaded with dye were rinsed thrice
408 (12,000 × g, 1 min) in RPMI-1640 culture medium, then resuspended in physiological saline
409 (as previously mentioned) with or without various concentrations of CIP. A 96-well microtiter
410 plate was filled with around 200 μL of parasite suspension per well. The dye-loaded cells
411 fluoresced at 520 nm after being stimulated at 440 and 490 nm. A pH calibration was carried
412 out for each experiment (Mohring et al., 2022).

413 **Measurements of membrane ATPase activity**

414 Membranes from isolated *B. gibsoni* were prepared by lysing the parasites in ice-cold
415 deionized water containing 7 × Protease Inhibitor Cocktail Tablets (Roche, Germany). The
416 membrane preparation was then washed three times with ice-cold deionized water, with
417 protease inhibitors included in the first two washes (Qiu et al., 2022). Protein concentrations
418 in the membrane samples were determined using a Bradford assay. The production of
419 inorganic phosphate (Pi) from ATP hydrolysis was measured using the Malachite Green
420 Phosphate Assay (BioAssay Systems, USA). Membrane preparations were diluted in either a
421 high Na^+ solution (final reaction conditions: 150 mM NaCl, 20 mM KCl, 2 mM $MgCl_2$, 50
422 mM Tris, pH 7.2) or a Na^+-free solution (final reaction conditions: 150 mM choline chloride,
423 20 mM KCl, 2 mM $MgCl_2$, 50 mM Tris, pH 7.2) to achieve a final protein concentration of

424 40 μg/mL. CIP was added at the concentrations specified in the respective figure legends.
425 Reactions were conducted according to the manufacturer's protocol provided with the assay
426 kit.

427 **Multiple ATP4 sequence alignment and molecular docking**

428 *B. gibsoni* ATP4 (GenBank: KAK1443404.1), *B. bovis* ATP4 (PiroplasmaDB:
429 BBOV_IV010020), *B. microti* ATP4 (GenBank: BMR1_03g01005), *T. gondii* ATP4
430 (GenBank: XP_018635122.1), and *Homo sapiens* ATP4 (GenBank: NM_000704.3)
431 sequences were obtained by a homology search using *P. falciparum* ATP4 (GenBank:
432 PF3D7_1211900). Sequence alignment was analyzed using MUSCLE in Jalview v2.11.3.2
433 software and BLAST (http://www.ncbi.nlm.nih.gov/BLAST/).

434 AlphaFold was used to predict the structure of *Bg*ATP4^{WT} (Jumper et al., 2021). Using the
435 GROMACS 2021 Molecular Dynamics package, the energy minimization was carried out
436 following the model's generation (Lindahl et al., 2021). The mutations were produced by
437 using Charmm-GUI PDB reader (Jo et al., 2014). PyMol (version 2.0 Schrödinger, LLC) was
438 used to confirm the position of the mutation site (center: -20.367, 10.904, 9.435; size:
439 30×30×30) (Trott and Olson, 2010). The ligand molecules CIP was downloaded from
440 PubChem (CID 44469321 (https://pubchem.ncbi.nlm.nih.gov/compound/ 44469321). The
441 ligand was used to dock with Gnina (Eberhardt et al., 2021). The affinity score and binding
442 pose were chosen only from the highest CNN (convolutional neural network) score results
443 from docking simulations. The models were visualized using the PyMOL Molecular Graphic
444 System and Discovery Studio.

445 **Cross-resistance to TQ and ATO in mutant parasites**

446 The efficacy of TQ and ATO against *Bg*ATP4^{WT}, *Bg*ATP4^{L921V}, and *Bg*ATP4^{L921I} was
447 evaluated using a fluorescence assay, as described above. The IC_{50} values were calculated
448 from the fluorescence values using non-linear regression analysis (curve fitting) in GraphPad

449 Prism 9 (GraphPad Software Inc., USA).

450 **Efficacy of CIP plus TQ combination therapy in SCID mice infected with *B. microti***

451 Twenty 6-week-old female immunocompromised mice (C.B-17/IcrJcl-Prkdcscid strain,
452 CLEA Japan, Inc.) were intraperitoneally injected with 1.0×10^7 of *B. microti*-infected blood
453 cells (Tuvshintulga et al., 2022). When the average parasitemia across all mice reached 1%
454 (at 4 DPI), the drug treatments were initiated. The CIP group (n = 5) was orally administered
455 20 mg/kg CIP for seven days. The TQ group (n = 5) was orally administered a single dose of
456 20 mg/kg TQ. The CIP plus TQ group (n = 5) received the combination treatment, following
457 the dosage and administration methods described above. The vehicle group (n = 5) orally
458 received 0.2 mL of sesame oil as the control. Thin blood smears were prepared every other
459 day and examined under a light microscope to determine parasitemia levels.

460 **qPCR analysis**

461 To further verify the presence or absence of *B. microti* DNA in treated SCID mice, real-time
462 quantitative PCR analysis was performed as described previously (Vydyam et al., 2024).
463 Briefly, genomic DNA was extracted from samples collected at 90 DPI and subjected to
464 qPCR analysis using SYBR Green I, targeting a highly conserved region of *Babesia*
465 mitochondrial genome (mtDNA). Primers used were: Bmic-F
466 5′-TTGCGATAGTAATAGATTTACTGC-3′ and B-lsu-R2
467 5′-TCTTAACCCAACTCACGTACCA-3′ (Qurollo et al., 2017). The reaction mixture
468 consisted of: 1 × Advanced Universal SYBR Green Super Mix (2 ×) (1725270; Bio-Rad); 0.5
469 μM of each primer, and 2 μl of genomic DNA.

470 **Detection of *B. microti* ATP4 gene mutations in relapsed infected SCID mice**

471 The genomic DNA of the mutant parasites was extracted and sequenced (Ji et al., 2022a). The
472 primer sets used for sequencing are listed in Table supplement 2. The single nucleotide
473 variants were confirmed by pairwise alignment to the *Bm*ATP4^{WT} sequence (GenBank:

BMR1_03g01005).

Statistical analysis

Data analysis, namely one-way analysis of variance (ANOVA) and two-tailed unpaired t-tests, was performed using GraphPad Prism (La Jolla, CA, USA) version 9. A P value of <0.05 was considered a statistically significant result.

Acknowledgments

This work was supported by a Grant-in-Aid for Scientific Research (22H0250906), the JSPS Core-to-Core program, both from the Ministry of Education, Culture, Sports, Science, and Technology of Japan, and a grant from the Strategic International Collaborative Research Project (JPJ008837) promoted by the Ministry of Agriculture, Forestry, and Fisheries of Japan, and International Science and Technology Cooperation Project of Hubei Province (2024EHA018).

Declaration of Competing Interest

The authors declare that they have no known competing financial interests or personal relationships that could have appeared to influence the work reported in this paper.

Author contributions

Hang Li, Investigation, Data curation, Formal analysis, Writing – original draft, Writing – review & editing; Shengwei Ji, Methodology, Investigation, Software, Validation; Nanang R. Ariefta, Methodology, Software, Formal analysis; Eloiza May S. Galon, Visualization, Writing – review & editing; Shimaa AES El-Sayed, Methodology, Visualization; Thom Do, Methodology, Investigation; Lijun Jia, Data curation, Visualization; Miako Sakaguchi,

499 Methodology, Visualization; Masahito Asada, Investigation, Visualization; Yoshifumi
500 Nishikawa, Methodology, Resources; Xin Qin, Methodology, Data curation; Mingming Liu,
501 Conceptualization, Methodology, Investigation, Resources, Data curation, Funding
502 acquisition, Supervision, Writing – review & editing; Xuenan Xuan, Conceptualization,
503 Methodology, Validation, Formal analysis, Supervision, Project administration, Writing –
504 review & editing.
505

506 **Ethics**

507 All animal experiments were performed according to the Guide for the Care and Use of
508 Laboratory Animals of Obihiro University of Agriculture and Veterinary Medicine, which
509 was also approved by the Committee on the Ethics of Animal Experiments at the Obihiro
510 University of Agriculture and Veterinary Medicine, Japan (permit numbers: animal
511 experiment, 22-145 and 23-132; DNA experiment, 2207 and 2208; pathogen, 202308 and
512 202306).
513

514 **References**

515 Almazán C, Scimeca RC, Reichard MV, Mosqueda J. 2022. Babesiosis and Theileriosis in
516 North America. *Pathogens* **11**:168. doi:10.3390/pathogens11020168
517 Ariefta NR, Pagmadulam B, Nihei C, Nishikawa Y. 2022. Sparsomycin exhibits potent
518 antiplasmodial activity *in vitro* and *in vivo*. *Pharmaceutics* **14**:544.
519 doi:10.3390/pharmaceutics14030544
520 Bork S, Yokoyama N, Matsuo T, Claveria FG, Fujisaki K, Igarashi I. 2003. Clotrimazole,
521 ketoconazole, and clodinafop-propargyl inhibit the *in vitro* growth of *Babesia bigemina*
522 and *Babesia bovis* (Phylum Apicomplexa). *Parasitology* **127**:311–315.
523 doi:10.1017/S0031182003003895
524 Carvalho LJM, Tuvshintulga B, Nugraha AB, Sivakumar T, Yokoyama N. 2020. Activities of
525 artesunate-based combinations and tafenoquine against *Babesia bovis in vitro* and *Babesia*
526 *microti in vivo*. *Parasites Vectors* **13**:362. doi:10.1186/s13071-020-04235-7
527 Chu CS, Freedman DO. 2019. Tafenoquine and G6PD: a primer for clinicians. *J Travel Med*

26:taz023. doi:10.1093/jtm/taz023

ClinicalTrials.gov [Internet]. Bethesda (MD): National Library of Medicine (US). Identifier NCT04675931, To evaluate efficacy, safety, tolerability and PK of intravenous cipargamin in participants with severe *Plasmodium falciparum* malaria; 2024 Feb 29 [cited 2024 Apr 9]. Available from: https://clinicaltrials.gov/study/NCT04675931

Das S, Bhatanagar S, Morrisey JM, Daly TM, Burns JM, Coppens I, Vaidya AB. 2016. Na^+ influx induced by new antimalarials causes rapid alterations in the cholesterol content and morphology of *Plasmodium falciparum*. *PLoS Pathog* **12**:e1005647. doi:10.1371/journal.ppat.1005647

Dennis ASM, Lehane AM, Ridgway MC, Holleran JP, Kirk K. 2018. Cell swelling induced by the antimalarial KAE609 (cipargamin) and other *Pf*ATP4-associated antimalarials. *Antimicrob Agents Chemother* **62**:e00087-18. doi:10.1128/AAC.00087-18

Diarra A, Sheldon C, Church J. 2001. In situ calibration and [H^+] sensitivity of the fluorescent Na^+ indicator SBFI. *American Journal of Physiology-Cell Physiology* **280**:C1623–C1633. doi:10.1152/ajpcell.2001.280.6.C1623

Eberhardt J, Santos-Martins D, Tillack AF, Forli S. 2021. AutoDock Vina 1.2.0: new docking methods, expanded force field, and python bindings. *J Chem Inf Model* **61**:3891–3898. doi:10.1021/acs.jcim.1c00203

Gray JS, Ogden NH. 2021. Ticks, human babesiosis and climate change. *Pathogens* **10**:1430. doi:10.3390/pathogens10111430

Guswanto A, Sivakumar T, Rizk MA, Elsayed SAE, Youssef MA, ElSaid EES, Yokoyama N, Igarashi I. 2014. Evaluation of a fluorescence-based method for antibabesial drug screening. *Antimicrob Agents Chemother* **58**:4713–4717. doi:10.1128/AAC.00022-14

Hidayati AR, Melinda, Ilmi H, Sakura T, Sakaguchi M, Ohmori J, Hartuti ED, Tumewu L, Inaoka DK, Tanjung M, Yoshida E, Tokumasu F, Kita K, Mori M, Dobashi K, Nozaki T, Syafruddin D, Hafid AF, Waluyo D, Widyawaruyanti A. 2023. Effect of geranylated dihydrochalcone from *Artocarpus altilis* leaves extract on *Plasmodium falciparum* ultrastructural changes and mitochondrial malate: Quinone oxidoreductase. *International Journal for Parasitology: Drugs and Drug Resistance* **21**:40–50. doi:10.1016/j.ijpddr.2022.12.001

Holbrook NR, Klontz EH, Adams GC, Schnittman SR, Issa NC, Bond SA, Branda JA, Lemieux JE. 2023. *Babesia microti* variant with multiple resistance mutations detected in an immunocompromised patient receiving atovaquone prophylaxi. *Open Forum Infectious Diseases* **10**:ofad097. doi:10.1093/ofid/ofad097

Hwang S-J, Yamasaki M, Nakamura K, Sasaki N, Murakami M, Wickramasekara Rajapakshage BK, Ohta H, Maede Y, Takiguchi M. 2010. Development and characterization of a strain of *Babesia gibsoni* resistant to diminazene aceturate *in vitro*. *J Vet Med Sci* **72**:765–771. doi:10.1292/jvms.09-0535

566 Jalovecka M, Sojka D, Ascencio M, Schnittger L. 2019. *Babesia* life cycle-when phylogeny
567 meets biology. *Trends in Parasitology* **35**:356–368. doi:10.1016/j.pt.2019.01.007
568 Jeon SA, Park JL, Park S-J, Kim JH, Goh S-H, Han J-Y, Kim S-Y. 2021. Comparison
569 between MGI and Illumina sequencing platforms for whole genome sequencing. *Genes*
570 *Genom* **43**:713–724. doi:10.1007/s13258-021-01096-x
571 Ji S, Galon EM, Rizk MA, Yi Y, Zafar I, Li H, Ma Z, Iguchi A, Asada M, Liu M, Xuan X.
572 2022a. Efficacy of the antimalarial MMV390048 against *Babesia* infection reveals
573 phosphatidylinositol 4-kinase as a druggable target for babesiosis. *Antimicrob Agents*
574 *Chemother* **66**:e00574-22. doi:10.1128/aac.00574-22
575 Ji S, Liu M, Galon EM, Rizk MA, Tuvshintulga B, Li J, Zafar I, Hasegawa Y, Iguchi A,
576 Yokoyama N, Xuan X. 2022b. Inhibitory effect of naphthoquine phosphate on *Babesia*
577 *gibsoni in vitro* and *Babesia rodhaini in vivo*. *Parasites Vectors* **15**:10.
578 doi:10.1186/s13071-021-05127-0
579 Jo S, Cheng X, Islam SM, Huang L, Rui H, Zhu A, Lee HS, Qi Y, Han W, Vanommeslaeghe
580 K, MacKerell AD, Roux B, Im W. 2014. CHARMM-GUI PDB manipulator for advanced
581 modeling and simulations of proteins containing nonstandard residues. *Adv Protein Chem*
582 *Struct Biol* **96:** 235–265. doi:10.1016/bs.apcsb.2014.06.002
583 Jumper J, Evans R, Pritzel A, Green T, Figurnov M, Ronneberger O, Tunyasuvunakool K,
584 Bates R, Žídek A, Potapenko A, Bridgland A, Meyer C, Kohl SAA, Ballard AJ, Cowie A,
585 Romera-Paredes B, Nikolov S, Jain R, Adler J, Back T, et al. 2021. Highly accurate protein
586 structure prediction with AlphaFold. *Nature* **596**:583–589.
587 doi:10.1038/s41586-021-03819-2
588 Kletsova EA, Spitzer ED, Fries BC, Marcos LA. 2017. Babesiosis in Long Island: review of
589 62 cases focusing on treatment with azithromycin and atovaquone. *Ann Clin Microbiol*
590 *Antimicrob* **16**:26. doi:10.1186/s12941-017-0198-9
591 Krause PJ. 2019. Human babesiosis. *International Journal for Parasitology* **49**:165–174.
592 doi:10.1016/j.ijpara.2018.11.007
593 Krause PJ, Auwaerter PG, Bannuru RR, Branda JA, Falck-Ytter YT, Lantos PM, Lavergne V,
594 Meissner HC, Osani MC, Rips JG, Sood SK, Vannier E, Vaysbrot EE, Wormser GP. 2021.
595 Clinical practice guidelines by the infectious diseases society of America (IDSA): 2020
596 guideline on diagnosis and management of babesiosis. *Clinical Infectious Diseases*
597 **72**:e49–e64. doi:10.1093/cid/ciaa1216
598 Krause PJ, Rogers R, Shah MK, Kang H, Parsonnet J, Kodama R, Vannier E. 2024.
599 Tafenoquine for relapsing babesiosis: a case series. *Clinical Infectious Diseases*
600 **79**:130–137. doi:10.1093/cid/ciae238
601 Krishna S, Woodrow C, Webb R, Penny J, Takeyasu K, Kimura M, East JM. 2001.
602 Expression and functional characterization of a *Plasmodium falciparum* $Ca2^{+}$-ATPase
603 (*Pf*ATP4) belonging to a subclass unique to apicomplexan organisms. *Journal of*

604 *Biological Chemistry* **276**:10782–10787. doi:10.1074/jbc.M010554200
605 Lee AH, Fidock DA. 2016. Evidence of a mild mutator phenotype in cambodian *Plasmodium*
606 *falciparum* malaria parasites. *PLoS ONE* **11**:e0154166. doi:10.1371/journal.pone.0154166
607 Lehane AM, Dennis ASM, Bray KO, Li D, Rajendran E, McCoy JM, McArthur HM,
608 Winterberg M, Rahimi F, Tonkin CJ, Kirk K, Van Dooren GG. 2019. Characterization of
609 the ATP4 ion pump in *Toxoplasma gondii*. *Journal of Biological Chemistry* **294**:5720–5734.
610 doi:10.1074/jbc.RA118.006706
611 Lemieux JE, Tran AD, Freimark L, Schaffner SF, Goethert H, Andersen KG, Bazner S, Li A,
612 McGrath G, Sloan L, Vannier E, Milner D, Pritt B, Rosenberg E, Telford S, Bailey JA,
613 Sabeti PC. 2016. A global map of genetic diversity in *Babesia microti* reveals strong
614 population structure and identifies variants associated with clinical relapse. *Nat Microbiol*
615 **1**:16079. doi:10.1038/nmicrobiol.2016.79
616 Li H, Galon EM, Ji S, Zafar I, Ma Z, Do T, Amer MM, Ma Y, Liu M, Xuan X. 2023. *In vitro*
617 screening of compounds from the Food and Drug Administration-approved library
618 identifies anti-*Babesia gibsoni* activity of idarubicin hydrochloride and vorinostat.
619 *Parasitology International* **96**:102774. doi:10.1016/j.parint.2023.102774
620 Lindahl, Abraham, Hess, Spoel VD. 2021. GROMACS 2021 Manual.
621 doi:10.5281/ZENODO.4457591
622 Liu M, Adjou Moumouni PF, Cao S, Asada M, Wang G, Gao Y, Guo H, Li J, Vudriko P,
623 Efstratiou A, Ringo AE, Lee S-H, Hakimi H, Masatani T, Sunaga F, Kawazu S, Yamagishi
624 J, Jia L, Inoue N, Xuan X. 2018. Identification and characterization of interchangeable
625 cross-species functional promoters between *Babesia gibsoni* and *Babesia bovis*. *Ticks and*
626 *Tick-borne Diseases* **9**:330–333. doi:10.1016/j.ttbdis.2017.11.008
627 Liu M, Galon EM, Ji S, Xuan X. 2024. Tafenoquine-based combination therapies: a step
628 toward babesiosis elimination. *The Journal of Infectious Diseases* **229**:1599–1600.
629 doi:10.1093/infdis/jiae083
630 Liu M, Ji S, Kondoh D, Galon EM, Li J, Tomihari M, Yanagawa M, Tagawa M, Adachi M,
631 Asada M, Igarashi I, Iguchi A, Xuan X. 2021. Tafenoquine is a promising drug candidate
632 for the treatment of babesiosis. *Antimicrob Agents Chemother* **65**:e00204-21.
633 doi:10.1128/AAC.00204-21
634 Marcos LA, Leung A, Kirkman L, Wormser GP. 2022. Use of tafenoquine to treat a patient
635 with relapsing babesiosis with clinical and molecular evidence of resistance to
636 azithromycin and atovaquone. *IDCases* **27**:e01460. doi:10.1016/j.idcr.2022.e01460
637 Matsuu A, Koshida Y, Kawahara M, Inoue K, Ikadai H, Hikasa Y, Okano S, Higuchi S. 2004.
638 Efficacy of atovaquone against *Babesia gibsoni in vivo* and *in vitro*. *Veterinary*
639 *Parasitology* **124**:9–18. doi:10.1016/j.vetpar.2004.07.005
640 Mohring F, Van Schalkwyk DA, Henrici RC, Blasco B, Leroy D, Sutherland CJ, Moon RW.
641 2022. Cation ATPase (ATP4) orthologue replacement in the malaria parasite *Plasmodium*

642 *knowlesi* reveals species-specific responses to ATP4-targeting drugs. *mBio* **13**:e01178-22.
643 doi:10.1128/mbio.01178-22
644 Ndayisaba G, Yeka A, Asante KP, Grobusch MP, Karita E, Mugerwa H, Asiimwe S, Oduro A,
645 Fofana B, Doumbia S, Jain JP, Barsainya S, Kullak-Ublick GA, Su G, Schmitt EK,
646 Csermak K, Gandhi P, Hughes D. 2021. Hepatic safety and tolerability of cipargamin
647 (KAE609), in adult patients with *Plasmodium falciparum* malaria: a randomized, phase II,
648 controlled, dose-escalation trial in sub-Saharan Africa. *Malar J* **20**:478.
649 doi:10.1186/s12936-021-04009-1
650 Qiu D, Pei JV, Rosling JEO, Thathy V, Li D, Xue Y, Tanner JD, Penington JS, Aw YTV, Aw
651 JYH, Xu G, Tripathi AK, Gnadig NF, Yeo T, Fairhurst KJ, Stokes BH, Murithi JM,
652 Kümpornsin K, Hasemer H, Dennis ASM, et al. 2022. A G358S mutation in the
653 *Plasmodium falciparum* Na^+ pump *Pf*ATP4 confers clinically-relevant resistance to
654 cipargamin. *Nat Commun* **13**:5746. doi:10.1038/s41467-022-33403-9
655 Qurollo BA, Archer NR, Schreeg ME, Marr HS, Birkenheuer AJ, Haney KN, Thomas BS,
656 Breitschwerdt EB. 2017. Improved molecular detection of *Babesia* infections in animals
657 using a novel quantitative real-time PCR diagnostic assay targeting mitochondrial DNA.
658 *Parasites Vectors* **10**:128. doi:10.1186/s13071-017-2064-1
659 Rogers R, Krause PJ, Norris AM, Ting MH, Nagami EH, Cilley B, Vannier E. 2023. Broad
660 antimicrobial resistance in a case of relapsing babesiosis successfully treated with
661 tafenoquine. *Clinical Infectious Diseases* **76**:741–744. doi:10.1093/cid/ciac473
662 Rosenblatt J, Leung A, Baneman E, Fuller R, Taimur S, Paniz-Mondolfi AE, Malone AK,
663 Kirkman L, Jacobs SE. 2021. Relapsed *Babesia microti* infection following allogeneic
664 hematopoietic cell transplantation in a patient with B-cell acute lymphoblastic leukemia:
665 case report and review of the literature. *Open Forum Infectious Diseases* **8**:ofab323.
666 doi:10.1093/ofid/ofab323
667 Rosling JEO, Ridgway MC, Summers RL, Kirk K, Lehane AM. 2018. Biochemical
668 characterization and chemical inhibition of *Pf*ATP4-associated Na^+-ATPase activity in
669 *Plasmodium falciparum* membranes. *Journal of Biological Chemistry* **293**:13327–13337.
670 doi:10.1074/jbc.RA118.003640
671 Rottmann M, McNamara C, Yeung BKS, Lee MCS, Zou B, Russell B, Seitz P, Plouffe DM,
672 Dharia NV, Tan J, Cohen SB, Spencer KR, González-Páez GE, Lakshminarayana SB, Goh
673 A, Suwanarusk R, Jegla T, Schmitt EK, Beck H-P, Brun R, et al. 2010. Spiroindolones, a
674 potent compound class for the treatment of malaria. *Science* **329**:1175–1180.
675 doi:10.1126/science.1193225
676 Saliba KJ, Kirk K. 1999. pH regulation in the intracellular malaria parasite, *Plasmodium*
677 *falciparum*. *Journal of Biological Chemistry* **274**:33213–33219.
678 doi:10.1074/jbc.274.47.33213
679 Schmitt EK, Ndayisaba G, Yeka A, Asante KP, Grobusch MP, Karita E, Mugerwa H, Asiimwe

680 S, Oduro A, Fofana B, Doumbia S, Su G, Csermak Renner K, Venishetty VK, Sayyed S,
681 Straimer J, Demin I, Barsainya S, Boulton C, Gandhi P. 2022. Efficacy of cipargamin
682 (KAE609) in a randomized, phase II dose-escalation study in adults in Sub-Saharan Africa
683 with uncomplicated *Plasmodium falciparum* malaria. *Clinical Infectious Diseases*
684 **74**:1831–1839. doi:10.1093/cid/ciab716
685 Simon MS, Westblade LF, Dziedziech A, Visone JE, Furman RR, Jenkins SG, Schuetz AN,
686 Kirkman LA. 2017. Clinical and molecular evidence of atovaquone and azithromycin
687 resistance in relapsed *Babesia microti* infection associated with rituximab and chronic
688 lymphocytic leukemia. *Clinical Infectious Diseases* **65**:1222–1225. doi:10.1093/cid/cix477
689 Spillman NJ, Allen RJW, McNamara CW, Yeung BKS, Winzeler EA, Diagana TT, Kirk K.
690 2013. Na^+ regulation in the malaria parasite *Plasmodium falciparum* involves the cation
691 ATPase *Pf*ATP4 and is a target of the spiroindolone antimalarials. *Cell Host & Microbe*
692 **13**:227–237. doi:10.1016/j.chom.2012.12.006
693 Tayebwa DS, Tuvshintulga B, Guswanto A, Nugraha AB, Batiha GE-S, Gantuya S, Rizk MA,
694 Vudriko P, Sivakumar T, Yokoyama N, Igarashi I. 2018. The effects of nitidine chloride
695 and camptothecin on the growth of *Babesia* and *Theileria* parasites. *Ticks and Tick-borne*
696 *Diseases* **9**:1192–1201. doi:10.1016/j.ttbdis.2018.04.019
697 Trott O, Olson AJ. 2010. AutoDock Vina: improving the speed and accuracy of docking with
698 a new scoring function, efficient optimization, and multithreading. *J Comput Chem*
699 **31**:455–461. doi:10.1002/jcc.21334
700 Tuvshintulga B, Sivakumar T, Nugraha AB, Ahedor B, Batmagnai E, Otgonsuren D, Liu M,
701 Xuan X, Igarashi I, Yokoyama N. 2022. Combination of clofazimine and atovaquone as a
702 potent therapeutic regimen for the radical cure of *Babesia microti* infection in
703 immunocompromised hosts. *The Journal of Infectious Diseases* **225**:238–242.
704 doi:10.1093/infdis/jiab537
705 Vannier E, Krause PJ. 2012. Human babesiosis. *N Engl J Med* **366**:2397–2407.
706 doi:10.1056/NEJMra1202018
707 Vega CA, Buening GM, Green TJ, Carson CA. 1985. *In vitro* cultivation of *Babesia bigemina*.
708 *Am J Vet Res* **46**:416–420.
709 Vydyam P, Pal AC, Renard I, Chand M, Kumari V, Gennaro JC, Mamoun CB. 2024.
710 Tafenoquine-atovaquone combination achieves radical cure and confers sterile immunity in
711 experimental models of human babesiosis. *The Journal of Infectious Diseases*
712 **229**:161–172. doi:10.1093/infdis/jiad315
713 Zhang R, Suwanarusk R, Malleret B, Cooke BM, Nosten F, Lau Y-L, Dao M, Lim CT, Renia
714 L, Tan KSW, Russell B. 2016. A basis for rapid clearance of circulating ring-stage malaria
715 parasites by the spiroindolone KAE609. *J Infect Dis* **213**:100–104.
716 doi:10.1093/infdis/jiv358
717 Zhou Y, Fomovska A, Muench S, Lai B-S, Mui E, McLeod R. 2014. Spiroindolone that

718 inhibits *Pf*ATPase4 is a potent, cidal inhibitor of *Toxoplasma gondii* tachyzoites *in vitro*
719 and *in vivo*. *Antimicrob Agents Chemother* **58**:1789–1792. doi:10.1128/AAC.02225-13
720

721 **Figure Legends**

722 **Figure 1. CIP demonstrates potent inhibition on *Babesia* spp.. (A)** and **(B)**
723 Dose-dependent growth curve of CIP on *B. bovis* and *B. gibsoni in vitro*. Each value
724 represents the mean ± standard deviation (SD) of three independent experiments carried out
725 in triplicate. IC_{50}: the half maximal inhibitory concentration. **(C)** Inhibitory effects of CIP and
726 atovaquone (ATO) plus azithromycin (AZI) on the proliferation of *B. microti* in BALB/c mice.
727 **(D)** Hematocrit (HCT) values in mice treated with CIP or ATO plus AZI compared with
728 vehicle-treated mice. **(E)** Inhibitory effects of CIP and ATO plus AZI on the proliferation of *B.*
729 *rodhaini* in BALB/c mice. **(F)** Survival rates of CIP-treated, ATO plus AZI-treated, and
730 vehicle-treated mice. The treatment time is shown by two-way arrows, and significant
731 differences ($P < 0.01$) between the drug-treated groups and the vehicle-treated control group
732 are indicated by asterisks. The data from one of six individual experiments are expressed as
733 means ± SD. *, $P < 0.05$; **, $P < 0.01$.

734

735 **Figure 2. Mutations in *Bg*ATP4 mediate CIP resistance. (A-C)** Representative sequencing
736 chromatogram of wild-type and resistant parasites from CIP-treated *B. gibsoni*. The resistant
737 parasite genomic DNA is extracted from blood samples after a 60 day-treatment. The
738 *Bg*ATP4 gene was amplified and sequenced using the DNA. **(D)** Genes of high-frequency
739 sequence variants detected by NGS. **(E)** Dose-dependent growth curve of $Bg\text{ATP4}^{WT}$,
740 $Bg\text{ATP4}^{L921V}$, and $Bg\text{ATP4}^{L921I}$ *in vitro*. Each value represents the mean ± standard deviation
741 (SD) of three independent experiments carried out in triplicate.

742

743 **Figure 3. Mechanistic basis for resistance to CIP conferred by the L921V and L921I**
744 **mutations in *Bg*ATP4. (A)** Untreated and CIP-treated parasite morphology after incubation

745 for 72 h. Scale bar: 5 μm. (**B**) Sizes of 100 parasites in two groups measured with ImageJ
746 software in panels A. Statistically significant differences between the means of variables
747 determined by t-test. ****, $P < 0.0001$. (**C**) TEM of untreated and CIP-treated parasite. N,
748 Nucleus; SB, spherical body; V, vacuole. Scale bar: 500 nm. (**D**) $[Na^+]_i$ concentrations after
749 addition of CIP in *Bg*ATP4^{WT} line. Representative traces from the experiment that highlight
750 the impact of adding 20 nM CIP (blue), 1 nM CIP (green), or 0 nM CIP (grey) on the
751 concentration $[Na^+]_i$ of the *Bg*ATP4^{WT} line. (**E**) Alkalinization of pH_i in *Bg*ATP4^{WT} line upon
752 addition of the ATP4 inhibitor. (**F**) Addition of 20 nM CIP to the wild-type and resistant
753 parasite lines results in different $[Na^+]_i$ concentrations. (**G**) Addition of 20 nM CIP to the
754 wild-type and resistant parasite lines results in different pH_i concentrations. Experiments were
755 performed in technical duplicates for at least three biological repeats. **(H)** Data acquired in
756 the low Na^+ condition (containing only the 2 mM Na^+ introduced upon addition of 1 mM
757 Na_2ATP) was subtracted from data obtained in the high Na^+ condition to determine the
758 ATPase activity related to the *Bg*ATP4 proteins. The results are presented as the average of
759 data from three independent tests. (**I**) Dose-dependent *Bg*ATP4-associated ATPase activity
760 curve of *Bg*ATP4^{WT}, *Bg*ATP4^{L921V}, and *Bg*ATP4^{L921I} *in vitro*. ATPase activity was determined
761 at pH 7.2 in the presence of 150 mM Na^+ and 1mM Na_2ATP. Each value represents the mean
762 ± standard deviation (SD) of three independent experiments carried out in triplicate. *, $P <$
763 0.05; **, $P < 0.01$.
764

765 **Figure 4. Binding sites proximal to *Bg*ATP4 residue 921 predicted by molecular docking.**
766 **(A)** The lowest energy poses for CIP were located in reference to the whole protein structure,
767 docking against the WT (green), L921V (yellow), and L921I (pink) mutant *Bg*ATP4. The side
768 chain of L921 is also shown in a red stick at its position. (**B-D**) The zoomed views of the
769 binding locations of CIP.

770

771 **Figure 5. Cross-resistance between ATO and TQ in resistant parasites and combination**
772 **therapy based on CIP plus TQ. (A)** Dose-dependent growth curve of *Bg*ATP4^{WT},
773 *Bg*ATP4^{L921V}, and *Bg*ATP4^{L921I} by ATO treatment *in vitro*. **(B)** Dose-dependent growth curve
774 of *Bg*ATP4^{WT}, *Bg*ATP4^{L921V}, and *Bg*ATP4^{L921I} by TQ treatment *in vitro.* Each value represents
775 the mean ± standard deviation (SD) of three independent experiments carried out in triplicate.
776 **(C)** Inhibitory effects of CIP plus TQ on the proliferation of *B. microti* in SCID mice. The
777 data are presented as the means from one of five independent experiments. **(D)** Parasite DNA
778 was detected by qPCR on genomic DNA extracted from blood collected from untreated and
779 treated SCID mice infected with *B. microti* at 90 DPI. A dotted grey line across the graph
780 represents the average cut-off Cq value. Cut-off Cq ≤ 35 was considered as positive, while Cq
781 > 35 or no amplification was considered as negative. Each sample was analyzed in duplicate,
782 and two independent experiments were conducted. NA indicates no amplification.

783 **Supplementary Materials**

784 **Figure supplement 1. Cytotoxicity assay of CIP on the Madin-Darby canine kidney**
785 **(MDCK) cells and human foreskin fibroblasts (HFF).** The MTP-500 microplate reader is
786 utilized to detect the absorbance at 450 nm. The results are displayed as the mean ± standard
787 deviation of three separate tests. CC_{50}: the 50% cytotoxic concentration.

788

789 **Figure supplement 2. Multiple sequence alignment of ATP4 in different species.** A
790 yellow square and arrow denotes the *Bg*ATP4 mutation site discovered in this investigation;
791 purple squares and arrows represent sites linked to *P. falciparum* CIP resistance, and a gray
792 square and arrow represents sites associated with *T. gondii*.

793

794 **Figure supplement 3. Binding sites for CIP found by Gnina search across the entire**
795 **surface of the protein.** (**A-C**) The binding space of WT, L921V, and L921I mutants in
796 *Bg*ATP4 are labeled in green, yellow and pink, respectively.

797

798 **Figure supplement 4. Proposed mechanism of inhibition of CIP on wild-type and mutant**
799 **parasite-infected erythrocytes.** CIP disrupts the *Bg*ATP4 function of wild-type parasites,
800 which causes a net influx of Na^+ and efflux of H^+ from the parasite. The osmotic load
801 imposed on the influx of Na^+ further brings about parasite swelling and internal alkalinization,
802 which are the main factors in *Babesia* death. Mutations in ATP4 minimize the susceptibility
803 to ATP4 inhibitors by recovering H^+ and Na^+ balance, as indicated by the dotted arrows.

804 **Supplemental Tables**

805 **Table supplement 1.** Primer sets of *B. gibsoni* ATP4

Gene	Primer (5'-3')
*Bg*ATP4-1F	ACGTAGTTGTCGAACATCTTACACCAATGC
*Bg*ATP4-1R	CAGAGGTAGCATAGTGAGATCGCCCCGA
*Bg*ATP4-2F	GAGATTGCAAGGTTTACGGATGAGTCTATGG
*Bg*ATP4-2R	ATGACAACGTCACCGGGTACAACACGCTTG
*Bg*ATP4-3F	GAAAAGCTTGCTCAAATGTCTTCACCGACAAC
*Bg*ATP4-3R	GTTTCTGGACGAGTTGGATCCTCATAACC
*Bg*ATP4-4F	AAATTGGGGGGGATAATTGGCATTATCTCC
*Bg*ATP4-4R	ACCTTATCAAAGGGTACCTCTTGCTTTG
*Bg*ATP4-5F	TCAATCCATTCGGTGGAATTTTCAAAAAGG
*Bg*ATP4-5R	GTGTTTGAATAACATATCTGGTGCCCCCTT
*Bg*ATP4-6F	GGTAAAGAACAGATTTGCTGACATAGATCT
*Bg*ATP4-6R	ACCCTATTTCTTGTGCGATGGCCGTAGCTG
*Bg*ATP4-7F	AGGGACGCTATAAATACTTGTGGAAAGGC
*Bg*ATP4-7R	GTACGCCCAGACTCGATTGAGTTAACTATTG
*Bg*ATP4-8F	GGGTATTAATGGCACAGATGTTGCAAAAGG
*Bg*ATP4-8R	GACAGTTCCCACTAGCATCATTAAGTGTAA
*Bg*ATP4-9F	ATCATCATTGCGCTATATGTTTCTACCGG
*Bg*ATP4-9R	CTAATGGGGTAGCATTTCCATTCTCAACAA
*Bg*ATP4-10F	AGGGAGTTCCTCCCATGTATAAAGATACCT
*Bg*ATP4 10R	TTAGGCTTCTGCCCTTTTCATTTTTCGCTT

806

807 **Table supplement 2.** Primer sets of *B. microti* ATP4

Gene	Primer (5'-3')
*Bm*ATP4-1F	ATGAGTAGATCTCAGTCTAACATTTC
*Bm*ATP4-1R	TGCTATTAGTAGTGCTATAACAAAG
*Bm*ATP4-2F	CAAGTATGGCGAAAATGCTATAAAC
*Bm*ATP4-2R	CATTCCGTTTGTTACGCTGGTGC
*Bm*ATP4-3F	CTTACAGGTGAGAGTGAAGATGTAAAG
*Bm*ATP4-3R	ACAAATTGCTGAGCAGCAACCCAGAG
*Bm*ATP4-4F	CTATTTCATTGTCATTGGGAGCTAA
*Bm*ATP4-4R	CAAATCCGGCCTTAGCTGCGCCAA
*Bm*ATP4-5F	TCATACGGTTCAACGTTATCACATG
*Bm*ATP4-5R	TCTATCCGACGACTCCAACCTTTC
*Bm*ATP4-6F	GTTGTCCAAGAATGCTTATAGGGTG
*Bm*ATP4-6R	CATTGCCACGCCAATGTCCGCCTGTTT
*Bm*ATP4-7F	GTTAACTCGTTGAAGAGACAAGGTTAC
*Bm*ATP4-7R	CACAATTGTACCGACAACTGCCGCTG
*Bm*ATP4-8F	GGCCAAAATCTCAGCCTTTAATGAC
*Bm*ATP4-8R	CAGCTCCAATGGGTTGGTAGTAACCATT
*Bm*ATP4-9F	CGTTATTGACGGCGTTGAGAATGATG
*Bm*ATP4-9R	CCCAAAACACCTTTGCCATTTAACTC
*Bm*ATP4-10F	GAAAATTGTAGAGCATTTCAAAACCAG
*Bm*ATP4 10R	TTATTGCAGGGCAGCCTGCTTAGA

808

809 **Table supplement 3.** Interactions of CIP from docking simulations

Receptor and binding energy	Name	Distance	Category	Types
*Bg*ATP4^{WT} -6.43 kcal/mol	GLY407	2.67648	Hydrogen Bond; Halogen	Carbon Hydrogen Bond; Halogen (Fluorine)
	CYS959	3.2396	Halogen	Halogen (Cl, Br, I)
	VAL962	2.66882	Hydrophobic	Pi-Sigma
	CYS959	4.38742	Hydrophobic	Alkyl
	VAL962	4.29249	Hydrophobic	Alkyl
	ALA963	3.8231	Hydrophobic	Alkyl
	ALA1202	3.67015	Hydrophobic	Alkyl
	MET211	5.06565	Hydrophobic	Alkyl
	VAL962	4.25668	Hydrophobic	Alkyl
	ILE414	4.70605	Hydrophobic	Alkyl
	CYS959	4.83891	Hydrophobic	Pi-Alkyl
	VAL962	4.98402	Hydrophobic	Pi-Alkyl
	VAL411	5.43239	Hydrophobic	Pi-Alkyl
	VAL962	5.05537	Hydrophobic	Pi-Alkyl
	PHE954	4.07586	Hydrophobic	Pi-Alkyl
*Bg*ATP4^{L921V} -6.40 kcal/mol	GLY407	2.69013	Hydrogen Bond; Halogen	Carbon Hydrogen Bond; Halogen (Fluorine)
	CYS959	3.22066	Halogen	Halogen (Cl, Br, I)
	VAL962	2.66391	Hydrophobic	Pi-Sigma
	CYS959	4.35422	Hydrophobic	Alkyl
	VAL962	4.31879	Hydrophobic	Alkyl
	ALA963	3.8209	Hydrophobic	Alkyl
	ALA1202	3.63038	Hydrophobic	Alkyl
	MET211	5.0878	Hydrophobic	Alkyl
	VAL962	4.24186	Hydrophobic	Alkyl
	ILE414	4.71819	Hydrophobic	Alkyl
	CYS959	4.82036	Hydrophobic	Pi-Alkyl
	VAL962	4.99879	Hydrophobic	Pi-Alkyl
	VAL411	5.4334	Hydrophobic	Pi-Alkyl
	VAL962	5.04532	Hydrophobic	Pi-Alkyl
	PHE954	4.07482	Hydrophobic	Pi-Alkyl
	GLY958	2.92346	Hydrogen Bond; Halogen	Carbon Hydrogen Bond; Halogen (Fluorine)
	GLY958	3.3301	Halogen	Halogen (Fluorine)
	MET410	5.88505	Other	Pi-Sulfur

	VAL955	4.31406	Hydrophobic	Alkyl
	MET410	3.69023	Hydrophobic	Alkyl
*Bg*ATP4^{L921I}	VAL411	4.83101	Hydrophobic	Alkyl
-6.26 kcal/mol	VAL955	4.79513	Hydrophobic	Alkyl
	VAL955	4.84729	Hydrophobic	Alkyl
	CYS959	4.1269	Hydrophobic	Alkyl
	ILE1205	4.82529	Hydrophobic	Alkyl
	CYS959	5.21399	Hydrophobic	Alkyl
	VAL955	4.90527	Hydrophobic	Pi-Alkyl
	PHE954	5.03012	Hydrophobic	Pi-Alkyl

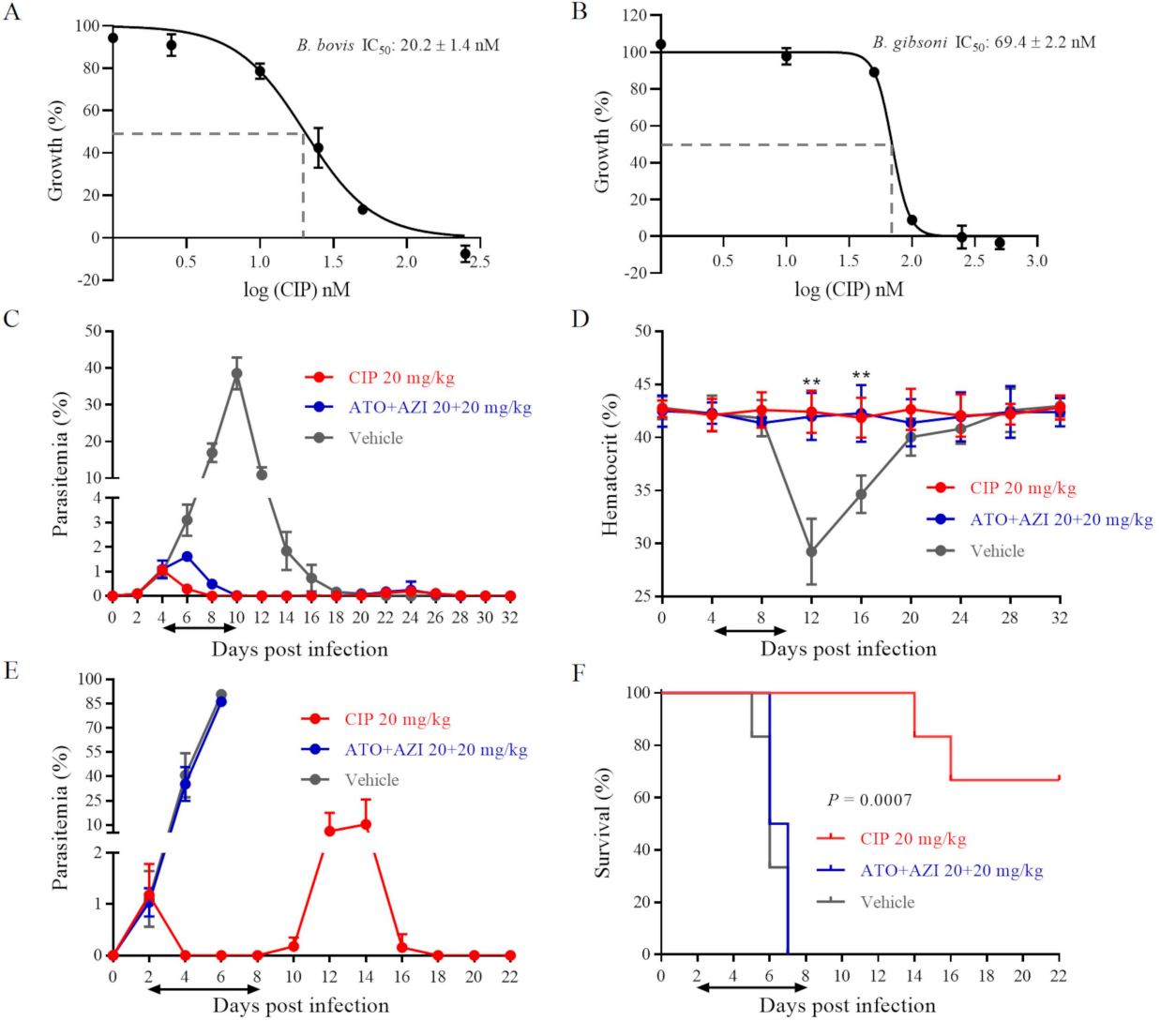
A
B. bovis IC50: 20.2 ± 1.4 nM
Growth (%)
log (CIP) nM
B
B. gibsoni IC50: 69.4 ± 2.2 nM
Growth (%)
log (CIP) nM
C
Parasitemia (%)
CIP 20 mg/kg
ATO+AZI 20+20 mg/kg
Vehicle
Days post infection
D
Hematocrit (%)
**
**
CIP 20 mg/kg
ATO+AZI 20+20 mg/kg
Vehicle
Days post infection
E
Parasitemia (%)
CIP 20 mg/kg
ATO+AZI 20+20 mg/kg
Vehicle
Days post infection
F
Survival (%)
P = 0.0007
CIP 20 mg/kg
ATO+AZI 20+20 mg/kg
Vehicle
Days post infection

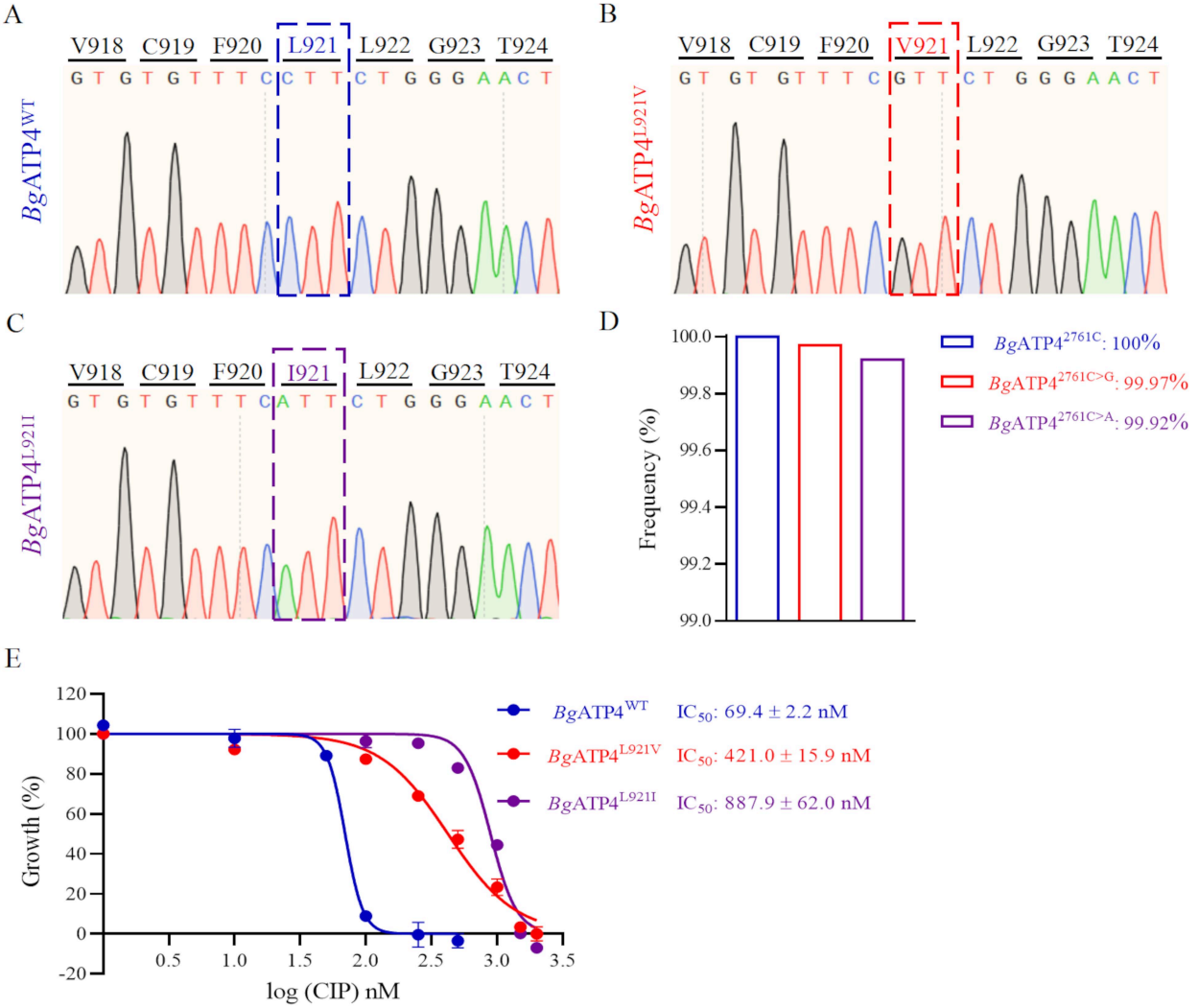
A
V918 C919 F920 L921 L922 G923 T924
G T G T G T T T C C T T C T G G G A A C T
BgATP4WT
B
V918 C919 F920 V921 L922 G923 T924
G T G T G T T T C G T T C T G G G A A C T
BgATP4L921V
C
V918 C919 F920 I921 L922 G923 T924
G T G T G T T T C A T T C T G G G A A C T
BgATP4L921I
D
Frequency (%)
100.0
99.8
99.6
99.4
99.2
99.0
BgATP42761C: 100%
BgATP42761C>G: 99.97%
BgATP42761C>A: 99.92%
E
Growth (%)
120
100
80
60
40
20
0
-20
0.5
1.0
1.5
2.0
2.5
3.0
3.5
log (CIP) nM
BgATP4WT IC50: 69.4 ± 2.2 nM
BgATP4L921V IC50: 421.0 ± 15.9 nM
BgATP4L921I IC50: 887.9 ± 62.0 nM

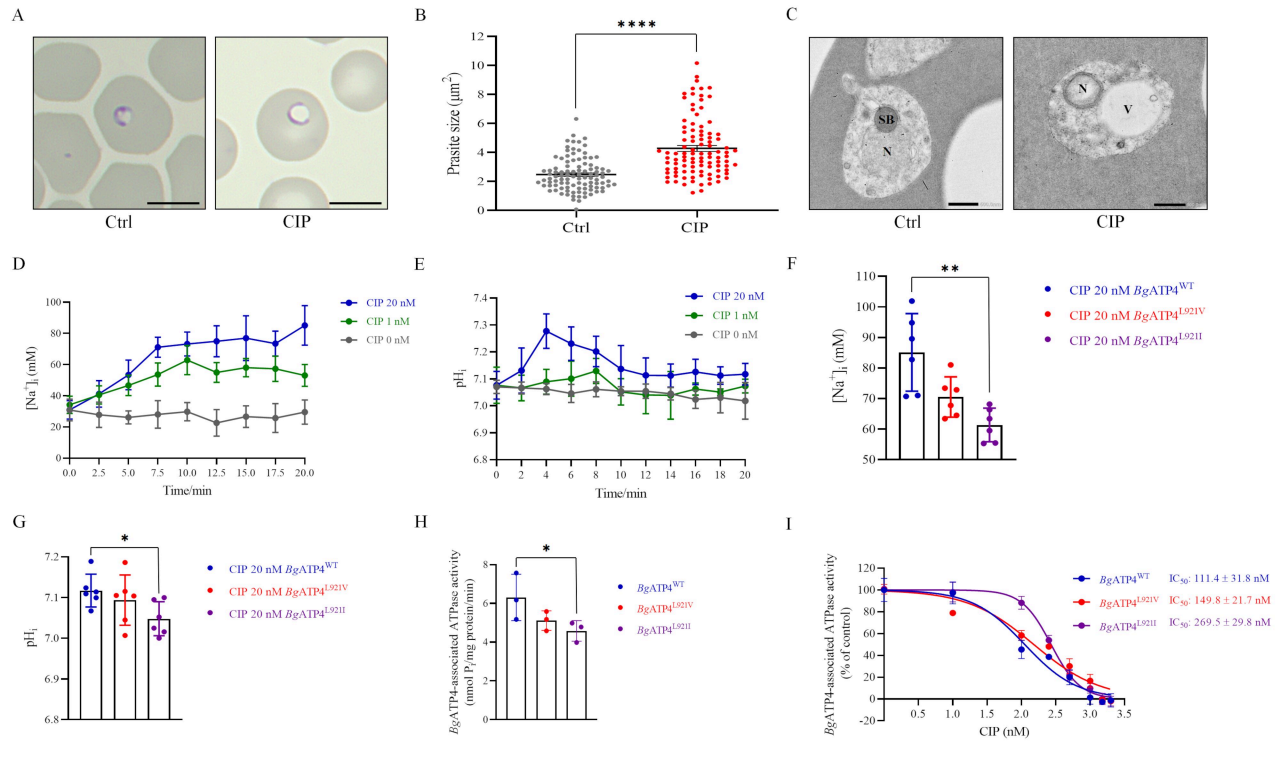
A
Ctrl
CIP
B
****
Prasite size (μm²)
Ctrl
CIP
C
SB
N
N
V
Ctrl
CIP
D
[Na⁺]i (mM)
Time/min
CIP 20 nM
CIP 1 nM
CIP 0 nM
E
pHi
Time/min
CIP 20 nM
CIP 1 nM
CIP 0 nM
F
**
[Na⁺]i (mM)
CIP 20 nM BgATP4WT
CIP 20 nM BgATP4L921V
CIP 20 nM BgATP4L921I
G
*
pHi
CIP 20 nM BgATP4WT
CIP 20 nM BgATP4L921V
CIP 20 nM BgATP4L921I
H
*
BgATP4-associated ATPase activity (nmol Pi/mg protein/min)
BgATP4WT
BgATP4L921V
BgATP4L921I
I
BgATP4-associated ATPase activity (% of control)
CIP (nM)
BgATP4WT IC50: 111.4 ± 31.8 nM
BgATP4L921V IC50: 149.8 ± 21.7 nM
BgATP4L921I IC50: 269.5 ± 29.8 nM

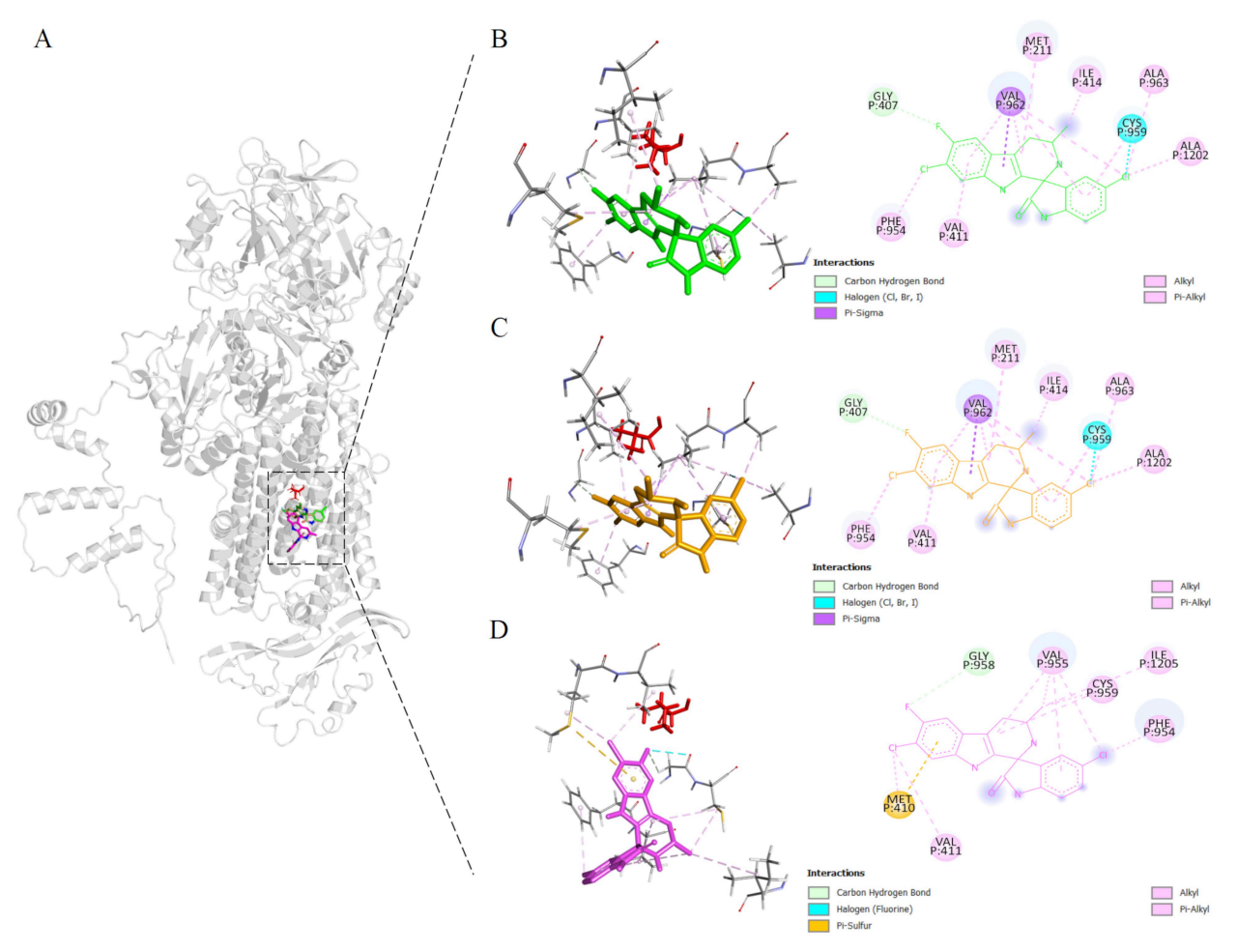
A
B
MET P:211
ILE P:414
ALA P:963
GLY P:407
VAL P:962
CYS P:959
ALA P:1202
PHE P:954
VAL P:411
Interactions
Carbon Hydrogen Bond
Halogen (Cl, Br, I)
Pi-Sigma
Alkyl
Pi-Alkyl
C
MET P:211
ILE P:414
ALA P:963
GLY P:407
VAL P:962
CYS P:959
ALA P:1202
PHE P:954
VAL P:411
Interactions
Carbon Hydrogen Bond
Halogen (Cl, Br, I)
Pi-Sigma
Alkyl
Pi-Alkyl
D
GLY P:958
VAL P:955
ILE P:1205
CYS P:959
PHE P:954
MET P:410
VAL P:411
Interactions
Carbon Hydrogen Bond
Halogen (Fluorine)
Pi-Sulfur
Alkyl
Pi-Alkyl

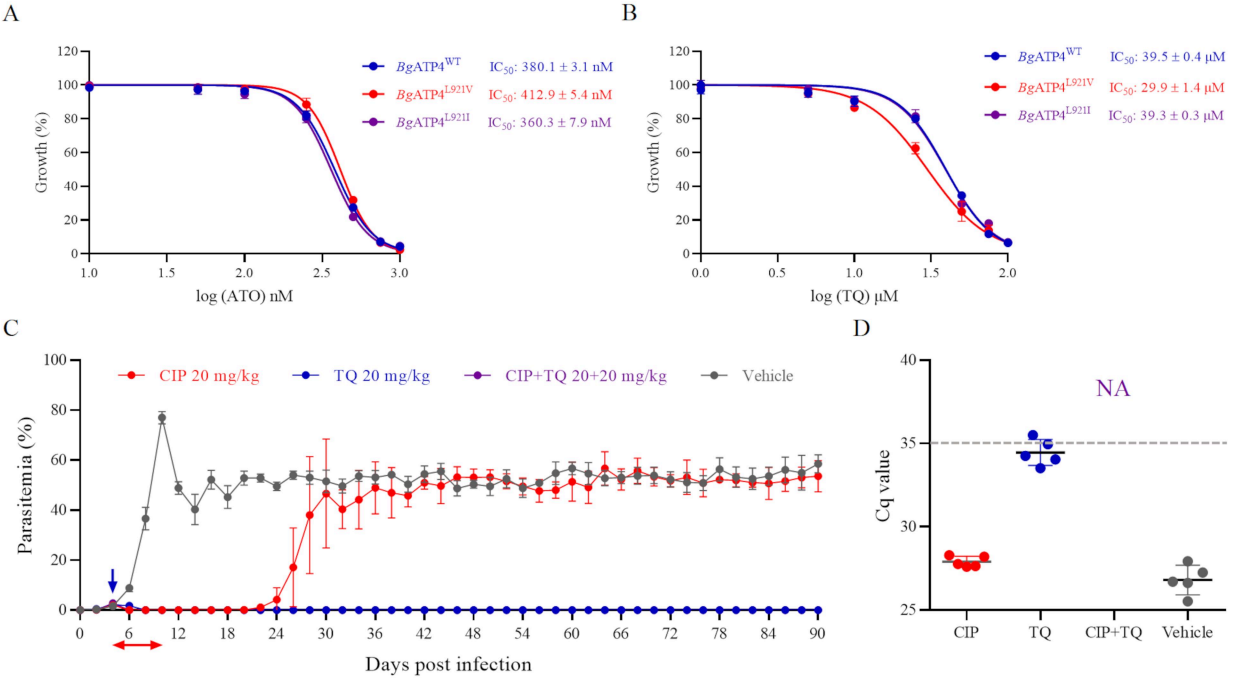
A
Growth (%)
log (ATO) nM
BgATP4WT IC50: 380.1 ± 3.1 nM
BgATP4L921V IC50: 412.9 ± 5.4 nM
BgATP4L921I IC50: 360.3 ± 7.9 nM
B
Growth (%)
log (TQ) μM
BgATP4WT IC50: 39.5 ± 0.4 μM
BgATP4L921V IC50: 29.9 ± 1.4 μM
BgATP4L921I IC50: 39.3 ± 0.3 μM
C
Parasitemia (%)
Days post infection
CIP 20 mg/kg
TQ 20 mg/kg
CIP+TQ 20+20 mg/kg
Vehicle
D
Cq value
NA
CIP
TQ
CIP+TQ
Vehicle

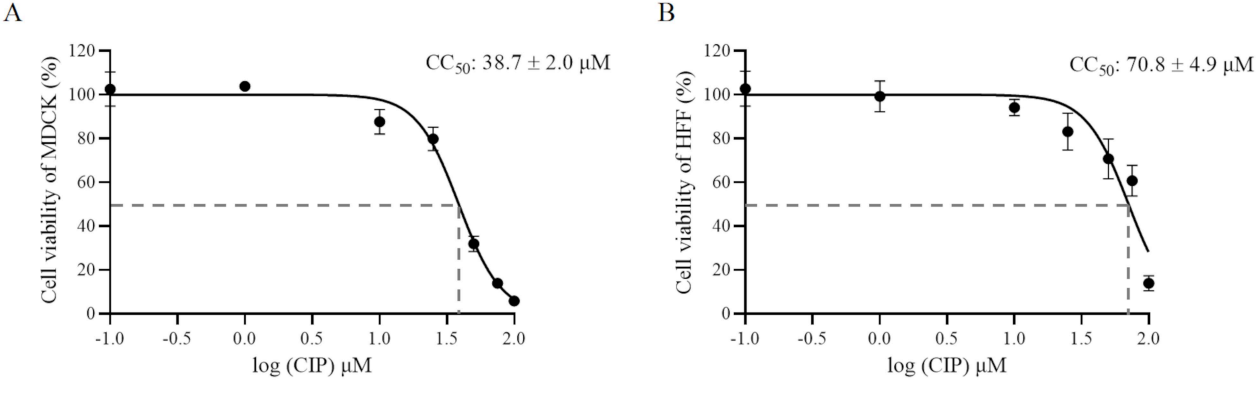
A
CC50: 38.7 ± 2.0 μM
Cell viability of MDCK (%)
120
100
80
60
40
20
0
-1.0
-0.5
0.0
0.5
1.0
1.5
2.0
log (CIP) μM
B
CC50: 70.8 ± 4.9 μM
Cell viability of HFF (%)
120
100
80
60
40
20
0
-1.0
-0.5
0.0
0.5
1.0
1.5
2.0
log (CIP) μM

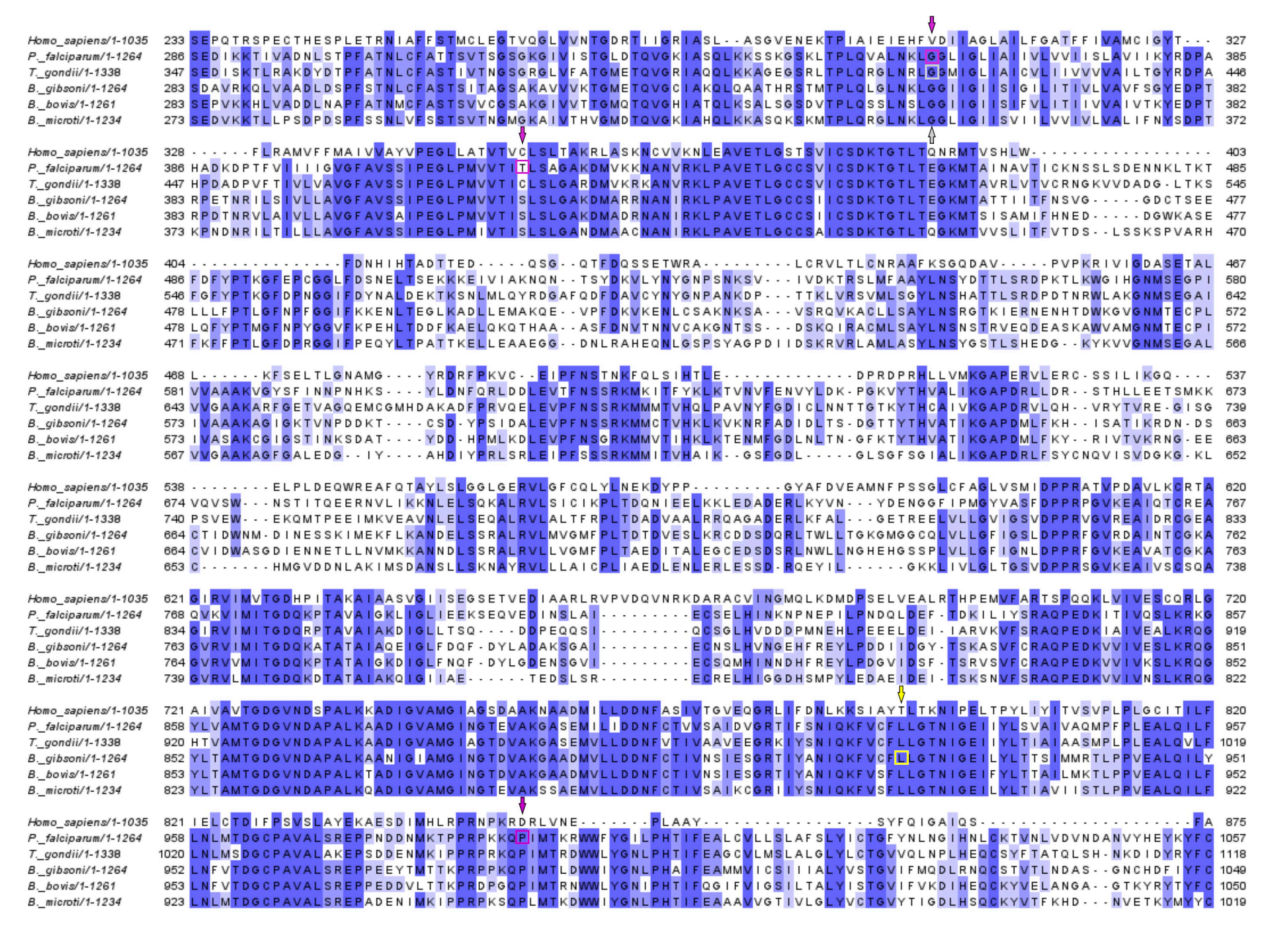
Homo_sapiens/1-1035
P._falciparum/1-1264
T._gondii/1-1338
B._gibsonii/1-1264
B._bovis/1-1261
B._microti/1-1234

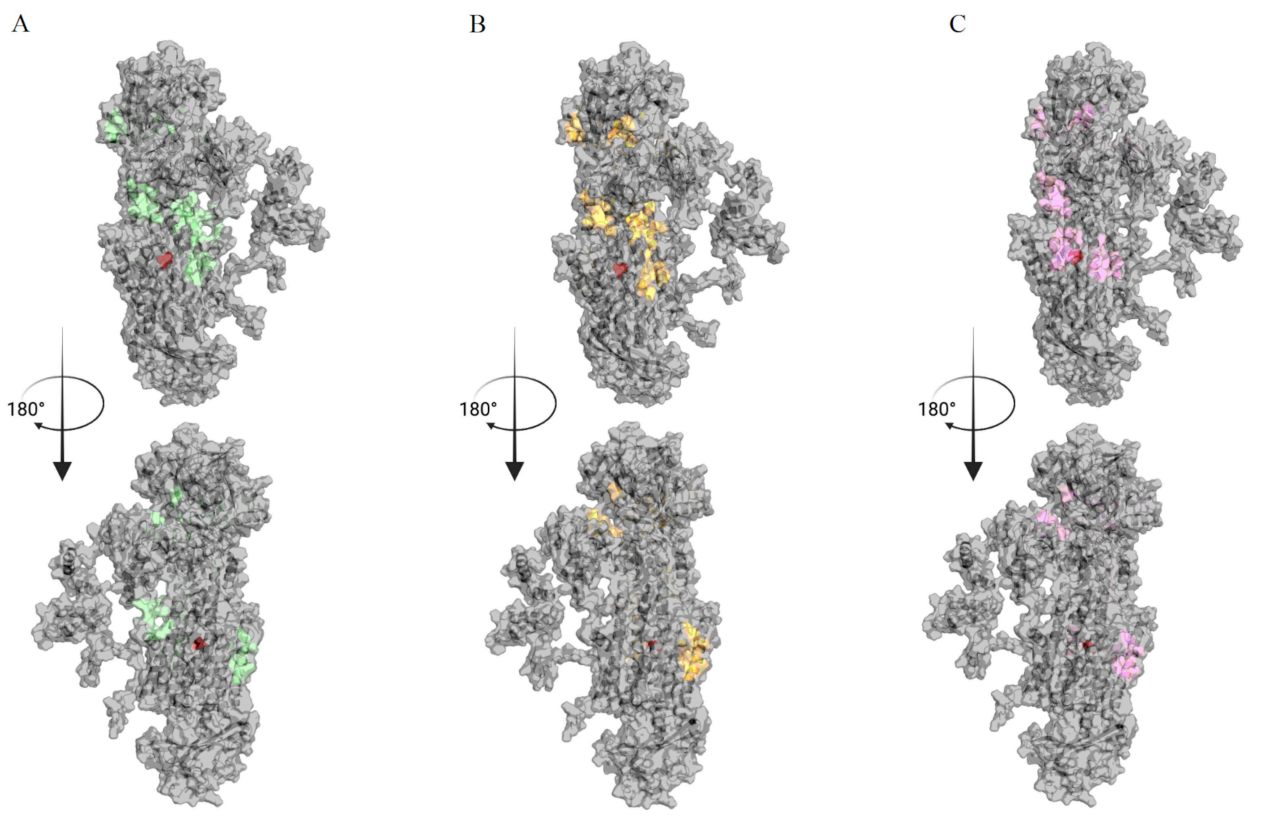
A
180°
B
180°
C
180°

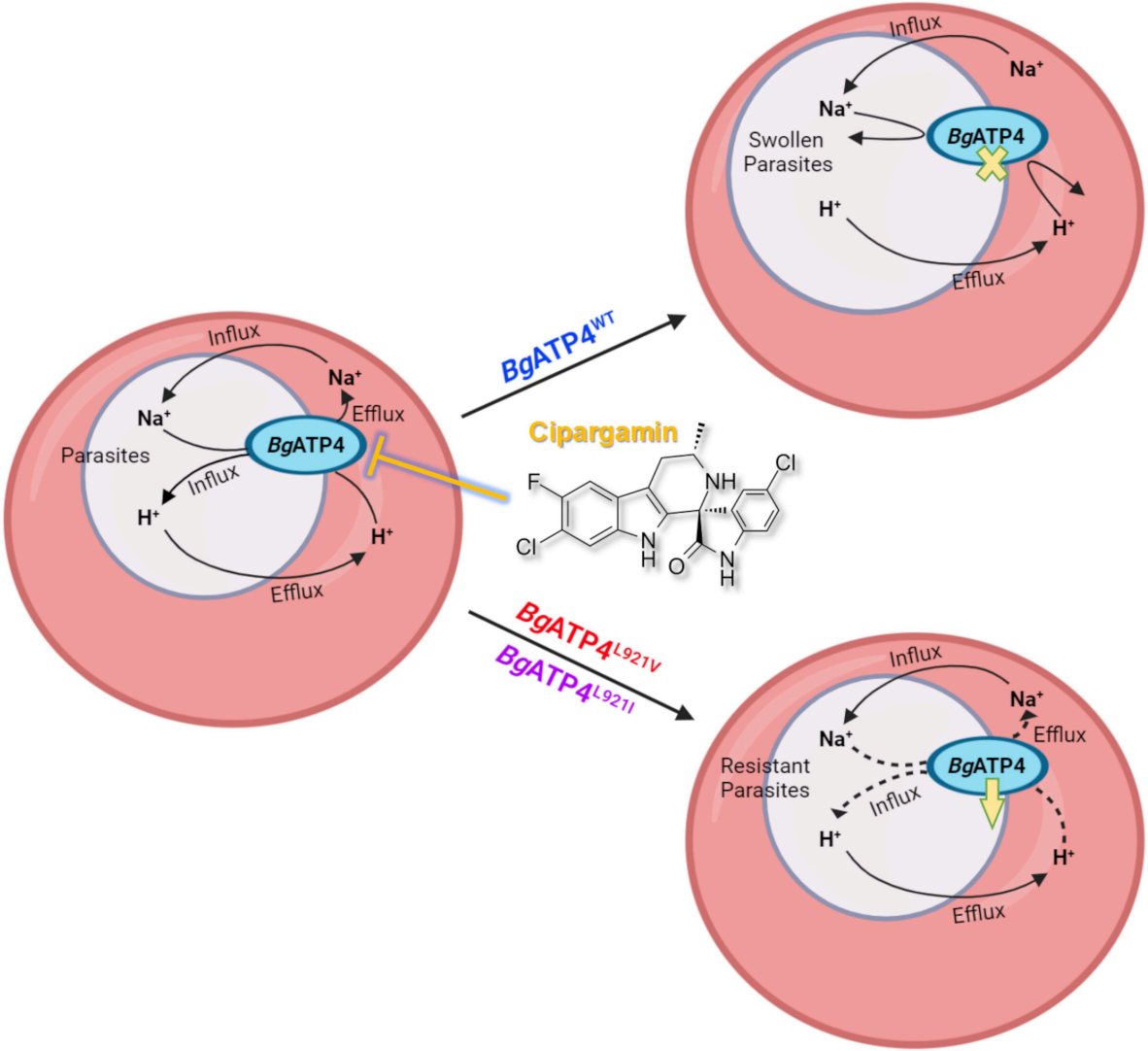
Influx
Na+
Na+
Swollen
Parasites
BgATP4
H+
H+
Efflux
BgATP4WT
Cipargamin
Influx
Na+
Na+
Efflux
Parasites
BgATP4
Influx
H+
H+
Efflux
F
Cl
NH
Cl
N
H
O
N
H
BgATP4L921V
BgATP4L921I
Influx
Na+
Na+
Efflux
Resistant
Parasites
BgATP4
Influx
H+
H+
Efflux